Detecting Elementary Particles

[The best reference for the physics of this lecture remains the book of Rossi.]

We can only observe directly those elementary particles which interact with a chunk of matter. As the bulk properties of matter are governed by electromagnetism it is not surprising that all particle detectors are based on the relatively low-energy electrical interactions of charged particles with matter. Detectors of neutral particles (photons, neutrons, neutrinos, ...) rely on a high energy interaction to convert the neutral particle into 2 n charged particles, which are really what is detected.

Interaction of a High Energy Charged Particle with Atoms

Long range electromagnetic interactions with the electrons and nucleus of an atom affect the high energy particle in two ways of interest:

- its energy is reduced;
- its motion is deflected.

As for the atom, the energy it absorbs goes almost entirely into the excitation and ionization of the electrons. Most particle detectors essentially observe these excited electrons.

We now give some semi-classical estimates of the excitation process.

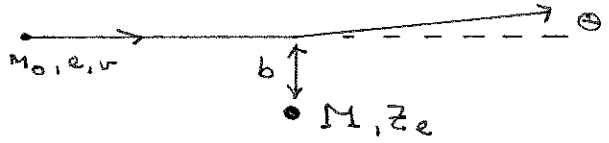

The maximum force on the moving charge is $F_{MAX} \approx Ze^2/b^2$

where b = impact parameter ≈ distance of closest approach

This force is applied for a characteristic time $\Delta t \sim \frac{2b}{v}$ = time that $F > \frac{F_{MAX}}{2}$

Thus an impulse $\Delta p \approx F_{MAX}\,\Delta t = \frac{2Ze^2}{bv}$ is transmitted between the two particles.

Exercise: In the limit $\Delta\theta \to 0$, show that this result is 'exact' by an application of Gauss' law

It is important to note that we get the same result on calculating the impulse on the target particle. The field of a moving charge is stronger, according to Einstein, so F_{MAX} on target $= \gamma Ze^2/b^2$.

But the field is Lorentz contracted along the direction of motion, so $\Delta t \sim \frac{2b}{\gamma v} \Rightarrow \Delta p$ as before!

THE MOVING CHARGE IS DEFLECTED BY ANGLE $\Delta\theta = \frac{\Delta p}{p} = \frac{2Ze^2}{b\gamma m_0 v^2}$

EXERCISE : COMPARE WITH GRAVITY. NOTE THAT WE MIGHT THINK OF A PHOTON AS THE LIMIT $m_0 \to 0$, $\gamma \to \infty$ BUT $E = m_0\gamma c^2$ = CONSTANT. THEN $\Delta\theta \to 0$ FOR DEFLECTION OF PHOTONS DUE TO A FORCE DERIVED FROM A 4-VECTOR POTENTIAL. WHAT IS THE RESULT FOR SCALAR AND TENSOR POTENTIALS? DO YOU HAVE TO KNOW ABOUT GENERAL RELATIVITY TO ANSWER THIS?

THE MOVING PARTICLE LOSES A SMALL AMOUNT OF ENERGY IN THE ABOVE INTERACTION, WHICH IS MORE READILY CALCULATED AS THE ENERGY GAIN OF THE TARGET PARTICLE. NAMELY

$$\Delta E = \frac{\Delta p^2}{2M} = \frac{2Z^2e^4}{Mb^2v^2}$$

IT IS INTERESTING TO COMPARE $\Delta\theta$ AND ΔE DUE TO SCATTERING OFF THE ELECTRONS OR THE NUCLEUS OF THE ATOM.

$$\Delta E_{\text{ELECTRON}} \sim Z \cdot \frac{e^4}{m_e} \quad \text{WHILE} \quad \Delta E_{\text{NUCLEUS}} \sim \frac{Z^2e^4}{M_{\text{NUCLEUS}}}$$

NOW $\frac{Z}{M_{\text{NUCLEUS}}} \ll \frac{1}{m_e}$ SO ENERGY IS LOST PRIMARILY TO SCATTERING OFF THE ELECTRONS. HOWEVER IN THE CASE OF $\Delta\theta$, THE Z SCATTERS OFF THE Z DIFFERENT ELECTRONS WILL BE IN DIFFERENT DIRECTIONS AND ADD UP TO A NET ANGLE $\sim \sqrt{Z}\,\Delta\theta$ ON AVERAGE (A RANDOM WALK PROCESS). SO SCATTERING OFF THE NUCLEUS IS MORE IMPORTANT IN DEFLECTING THE MOVING CHARGE.

ENERGY LOSS PER GRAM / CM^2

WE SKETCH AN ARGUMENT TO ESTIMATE THE TOTAL ENERGY LOST TO ATOMIC ELECTRONS BY A FAST CHARGED PARTICLE TRAVERSING A BLOCK OF MATERIAL. IT IS CUSTOMARY TO MEASURE THE THICKNESS OF THE MATERIAL NOT IN CM, BUT IN GRAMS / CM^2 = LENGTH / DENSITY. THEN

ΔE_{TOTAL} = (# OF ELECTRONS IN THICKNESS Δx) · (ENERGY LOSS TO AN ELECTRON)

$$\#\text{ OF } e\text{'S} = \frac{N_0}{A} \cdot Z \cdot \Delta x$$

N_0 = AVAGADRO'S NUMBER
A = ATOMIC NUMBER

WE FOUND THE ENERGY LOSS TO AN ELECTRON IF THE IMPACT PARAMETER IS b. THE PROBABILITY OF THIS IS JUST $2\pi b\,db$ / 1 CM^2

ALTOGETHER $$\frac{dE}{dx} = \frac{N_0}{A} Z \int_{b_{MIN}}^{b_{MAX}} 2\pi b\,db \cdot \frac{2Z^2e^4}{m_e b^2 v^2} = 4\pi \frac{N_0}{A} Z \frac{e^4}{m_e v^2} \ln\left(\frac{b_{MAX}}{b_{MIN}}\right)$$

THERE ARE LIMITS ON THE RANGE OF IMPACT PARAMETER b WHICH CAN CONTRIBUTE TO THE ENERGY LOSS.

FROM HEISENBERG WE LEARN $b_{MIN} P_{CM} \sim \hbar$

b IS TRANSVERSE TO p SO THIS MAY AT FIRST SEEM AN UNUSUAL APPLICATION OF THE UNCERTAINTY RULES. BUT bp = ANGULAR MOMENTUM, WHICH WILL HAVE AN UNCERTAINTY $\sim \hbar$ FOR INITIAL STATES NOT PREPARED WITH DEFINITE L, AS IN SHOOTING A PARTICLE INTO A BLOCK!

FOR A COLLISION WITH AN ELECTRON, $v_{CM} \sim v$, AND P_{CM} = C.M. MOMENTUM OF THE ELECTRON $= m_e \gamma_{CM} v_{CM} \sim m_e \gamma v$

$$\text{HENCE} \qquad b_{MIN} \sim \frac{\hbar}{m_e \gamma v}$$

ON THE OTHER HAND, IF b IS TOO LARGE, THE IMPULSE IS APPLIED SO SLOWLY THAT THE ELECTRON DOES NOT ACT INDEPENDENTLY OF THE REST OF THE ATOM. THE ATOM AS A WHOLE RECOILS, ABSORBING NEGLIGIBLE ENERGY (DUE TO ITS HIGH MASS).

THAT IS, WE SUPPOSE $\Delta t_{MAX} \sim \frac{2 b_{MAX}}{\gamma v} \lesssim \tau_{\text{ELECTRON IN ORBIT}}$

THE FACTOR $1/\gamma$ OCCURS BECAUSE OF THE LORENTZ CONTRACTION OF THE FIELD OF THE MOVING CHARGED, NOTED ABOVE.

NOW $\tau = \frac{1}{\nu} \sim \frac{h}{I}$ WHERE ν = FREQUENCY

$I = \langle h\nu \rangle$ = AVERAGE ELECTRON BINDING ENERGY $\equiv$ <u>IONIZATION POTENTIAL</u>

THUS $b_{MAX} \sim \frac{\gamma h v}{2 I}$

AND $$\frac{dE}{dx} \sim 4\pi \frac{N_0}{A} z \frac{e^4}{m_e v^2} \ln\left(\pi \frac{m_e \gamma^2 v^2}{I}\right)$$

COMPARE TO THE BETHE-BLOCH RESULT $4\pi \frac{N_0}{A} z \frac{e^4}{m_e v^2} \left(\ln \frac{2 m_e \gamma^2 v^2}{I} - \frac{2v^2}{c^2}\right)$

$\frac{dE}{dx}$ FALLS LIKE $\frac{1}{v^2}$ IF $v \ll c \Leftrightarrow \gamma \sim 1$; REACHES A BROAD MINIMUM AT $\gamma \sim 3$–4; AND RISES SLOWLY FOR $\gamma > 4$ – THE <u>RELATIVISTIC RISE</u>. A PARTICLE WITH $\gamma \sim 3$ TO 4 IS CALLED A <u>MINIMUM IONIZING PARTICLE</u>. $dE/dx \sim$ <u>1–2 MeV</u> PER GM/cm^2 AT MINIMUM. SEE TABLES APPENDED TO THIS LECTURE.

AT VERY SMALL VELOCITIES OUR EXPRESSION DIVERGES. HOWEVER THE WHOLE DERIVATION DOESN'T MAKE MUCH SENSE IF $v_{FAST} < v_{ATOMIC\ ELECTRONS} \sim c/100$. THE VERY LOW VELOCITY LIMIT HAS BECOME OF INTEREST LATELY BECAUSE OF MAGNETIC MONOPOLE SEARCHES. (SEE DRELL ET AL. PHYS. REV. LETT. 50, 644 (1983)).
[EXCERCISE: WHAT IS THE dE/dx LOSS FOR A MAGNETIC MONOPOLE MOVING THRU MATTER, IF $v/c > 1/100$?]

THE FIGURES SHOW CALCULATED AND OBSERVED dE/dx LOSS CURVES IN ARGON GAS.

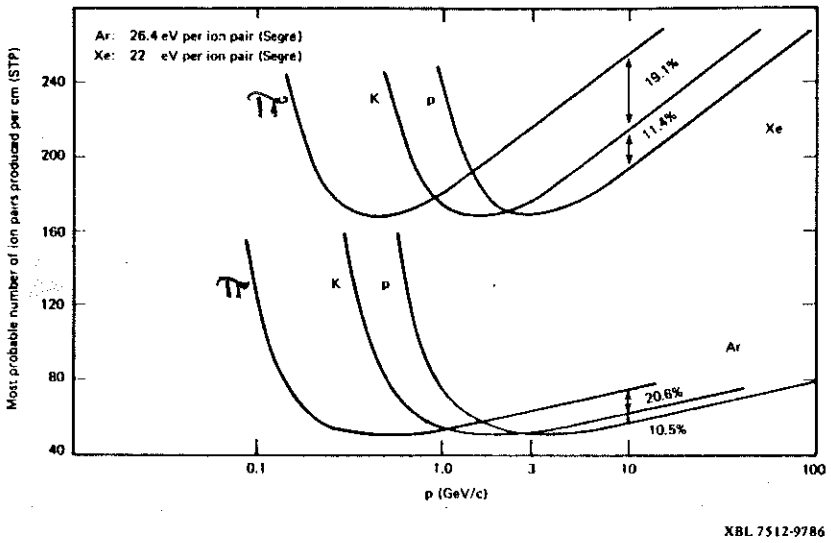

Fig. 11. The most probable number of ion pairs/cm for argon and xenon at STP, as a function of P(GeV/c) for pions, kaons, and protons. Not shown are the curves for electrons, which would be essentially flat at the asymptotic values goverened by the density effect.

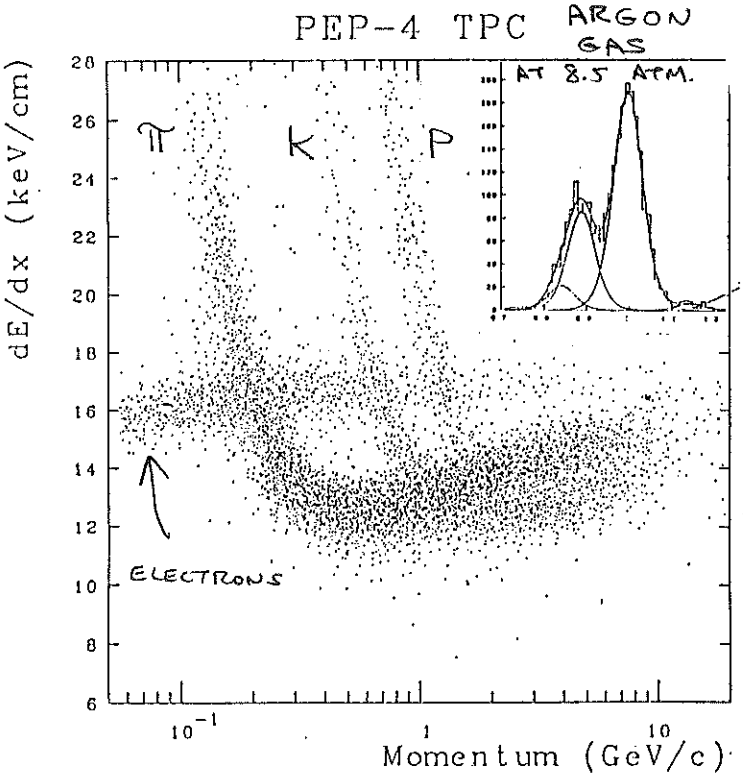

THIS INDICATES THE POSSIBILITY OF DETERMINING THE PARTICLE'S MASS (ASSUMING CHARGE = e) BY A MEASUREMENT OF MOMENTUM p AS WELL AS dE/dx. THIS IS BARELY POSSIBLE FOR $\gamma > 4$ DUE TO THE RELATIVISTIC RISE. BUT FOR $v \ll c$ SUCH MASS IDENTIFICATION IS READILY ACHIEVED, AND IN FACT THE FIRST ESTIMATES OF THE π AND K MESON MASSES CAME FROM dE/dx MEASUREMENTS OF TRACKS IN NUCLEAR EMULSIONS.

THE RELATIVISTIC RISE OCCURS BOTH BECAUSE b_{MAX} INCREASES AND b_{MIN} DECREASES AS $\gamma \to \infty$. THE FORMER CAN BE ATTRIBUTED TO THE RELATIVISTIC GROWTH OF THE ELECTRIC FIELD OF A MOVING CHARGE. HOWEVER, ONCE b_{MAX} BECOMES LARGER THAN THE INTER-ATOMIC SPACING, ONE ATOM SHIELDS ANOTHER, AND dE/dx DOES NOT INCREASE FURTHER — THE DENSITY EFFECT. SO THE RISE IS MUCH MORE PROMINENT IN GASES THAN IN SOLIDS OR LIQUIDS. PART OF THE RELATIVISTIC RISE IS ASSOCIATED WITH COHERENT RESPONSE OF THE MATERIAL TO THE ELECTRIC FIELD OF THE MOVING CHARGE: THE ČERENKOV EFFECT DISCUSSED BELOW.

Roughly one half the energy deposited goes into ionizing electrons. The rest merely excites the atoms to higher bound states. These may de-excite by photon emission causing scintillation light.

In most materials one electron is ionized for each 25-35 eV deposited. However, many of these ionizations are not directly due to the field of the moving charge. An electron ejected by the effect of the moving charge (primary ionization) typically carries away enough kinetic energy to cause 2-3 additional ionizations. The so-called δ-rays are just very energetic primary ionization electrons. We found $E \sim 1/b^2$ for these electrons. The probability of impact parameter b is $\sim 2\pi b\,db$, which then yields $P(E)\,dE \sim dE/E^2$ as the δ-ray energy spectrum. The fluctuations about the mean energy deposition due to δ-rays has been studied by Vavilov and Landau, and lead to a non-Gaussian distribution.

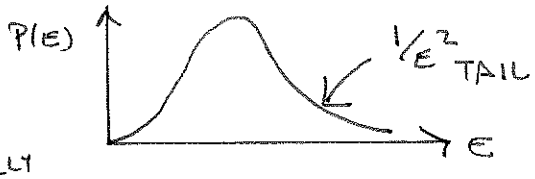

As usual with statistical processes the more samples taken (more primary ionization = thicker material), the more nearly Gaussian the total energy loss distribution becomes.

Multiple Coulomb Scattering

As well as losing energy while traversing material, a high energy charged particle suffers many small deflections, due mainly to Coulomb scattering off the nucleus. We found

$$\Delta\theta(b) \sim \frac{2Ze^2}{b\gamma m_0 v^2}$$

It is amusing to note that this quickly leads to the Rutherford scattering formula at small angles.

$$d\sigma = 2\pi b\,db = 2\pi \cdot \frac{4Z^2e^4}{\gamma^2 m_0^2 v^4}\,\frac{d\theta}{\theta^3} \quad \text{or} \quad \frac{d\sigma}{2\pi\theta\,d\theta} = \frac{d\sigma}{d\Omega} = \frac{Z^2e^4}{4(pv)^2(\theta/2)^4}$$

An interesting quantity is the total change in angle after many Coulomb interactions $\equiv \theta_0$. As many scatters occur to the left as right, up or down, so $\theta_0 = 0$ on average. But $\langle\theta_0^2\rangle$ will be non-vanishing. It grows with the thickness of material traversed, as in a random walk. That is,

$$\langle\theta_0^2\rangle = \delta\theta^2 z \qquad z = \text{thickness in gm/cm}^2\text{, say.}$$

where $\delta\theta^2 = \dfrac{d\langle\theta_0^2\rangle}{dz}$ = change in θ^2 while crossing unit thickness

so $\delta\theta^2 = \int \theta^2 P(\theta)\,d\Omega \approx 2\pi\int \theta^3 P(\theta)\,d\theta$ as small angles dominate.

$P(\theta)$ = PROB OF SCATTERING BY θ IN A SINGLE COLLISION • # OF NUCLEI PER GM/CM^2

$$= \frac{N_0}{A} \cdot \left.\frac{d\sigma}{d\Omega}\right|_{\text{RUTHERFORD}} = \frac{N_0}{A}\left(\frac{Ze^2}{pv}\right)^2 \frac{4}{\theta^4}$$

AND $$\delta\theta^2 = 8\pi \frac{N_0}{A}\left(\frac{Ze^2}{pv}\right)^2 \int \frac{d\theta}{\theta} = 8\pi \frac{N_0}{A}\left(\frac{Ze^2}{pv}\right)^2 \ln\left(\frac{\theta_{MAX}}{\theta_{MIN}}\right)$$

AS BEFORE, THERE ARE LIMITS TO THE PLAUSIBLE RANGE OF SCATTERING.

RECALL THAT $\theta \sim 1/b$ SO $\frac{\theta_{MAX}}{\theta_{MIN}} = \frac{b_{MAX}}{b_{MIN}}$. WE NEED THE RELEVANT LIMITS ON THE IMPACT PARAMETER FOR NUCLEAR COULOMB SCATTERING.

b_{MAX} ~ RADIUS OF ATOM ; OTHERWISE THE ELECTRONS SCREEN THE NUCLEUS

~ $\frac{\text{BOHR RADIUS}}{Z^{1/3}}$ IN THE THOMAS-FERMI MODEL ~ $\frac{r_e}{\alpha^2 Z^{1/3}}$ $\left(r_e = \frac{e^2}{M_e c^2}\right)$

b_{MIN} ~ RADIUS OF NUCLEUS ~ $A^{1/3} \cdot 1\,\text{FERMI}$

$$\frac{b_{MAX}}{b_{MIN}} \sim \frac{r_e}{(ZA)^{1/3}\alpha^2 \cdot 1\,\text{FERMI}} \sim \frac{2.8(137)^2}{Z^{2/3}Z^{2/3}} \sim \left(\frac{200}{Z^{1/3}}\right)^2$$

$$\delta\theta^2 \sim 16\pi \frac{N_0}{A} Z^2 \left(\frac{e^2}{p\beta c}\right)^2 \ln\left(\frac{200}{Z^{1/3}}\right)$$

THIS IS COMMONLY REWRITTEN AS

$$\delta\theta^2 = \underbrace{4\alpha \frac{N_0}{A} Z^2 \left(\frac{e^2}{M_e c^2}\right)^2 \ln\left(\frac{183}{Z^{1/3}}\right)}_{\equiv 1/X_0} \cdot \underbrace{\frac{4\pi}{\alpha}(M_e c)^2}_{(21\ \text{MeV})^2} \left(\frac{1}{p\beta}\right)^2$$

$X_0 \equiv$ RADIATION LENGTH, A CHARACTERISTIC PROPERTY OF THE MATERIAL.

THEN $$\langle\theta_0^2\rangle = \left(\frac{21\ \text{MeV}/c}{p\beta}\right)^2 \frac{z}{X_0} \qquad \theta_{0\,RMS} = \frac{21}{p\beta}\sqrt{\frac{z}{X_0}}$$

IT IS OFTEN MORE NATURAL TO DEAL IN THE PROJECTED SCATTERING ANGLE ONTO THE X-Z AND Y-Z PLANES.

NO $\langle\theta_x^2\rangle + \langle\theta_y^2\rangle = \langle\theta_0^2\rangle$ SO $\theta_x = \theta_y = \frac{15}{p\beta}\sqrt{\frac{z}{X_0}}$

FOR p MEASURED IN MeV/c.

AS THE PARTICLE'S ANGLE CHANGES DUE TO MULTIPLE COULOMB SCATTERING, A NET TRANSVERSE DISPLACEMENT IS GENERATED, ALSO BY A RANDOM WALK PROCESS. CAN YOU SHOW THAT

$$\Delta x = \Delta y = \sqrt{\langle y^2 \rangle} = \frac{1}{\sqrt{3}} \theta_y z$$ BY STATISTICAL CONSIDERATION?

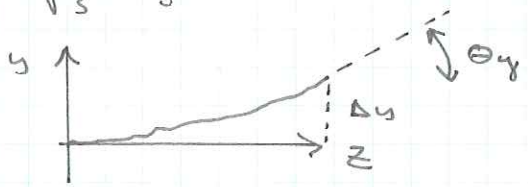

Δy AND θ_y, ETC. OBEY APPROXIMATE GAUSSIAN DISTRIBUTIONS, WITH STANDARD DEVIATIONS BEING THE QUANTITIES DERIVED ABOVE. HOWEVER, THERE ARE LONG NON-GAUSSIAN TAILS DUE TO OCCASIONAL VERY HARD NUCLEAR SCATTERINGS NOT WELL DESCRIBED BY TAKING b_{MIN} AS ABOVE.

WE NOW CONSIDER VARIOUS DETECTORS IN COMMON USE.

SCINTILLATION DETECTORS

WE INDICATED ABOVE THAT ABOUT 1/2 THE ENERGY DEPOSITED IN A BLOCK OF MATERIAL BY A PASSING CHARGED PARTICLE GOES INTO EXCITATION OF THE ATOMS TO HIGHER ELECTRONIC LEVELS. MOST EXCITED ATOMS HAVE REASONABLE PROBABILITY TO DE-EXCITE BY EMISSION OF A PHOTON (RATHER THAN, SAY, TRANSFERRING ENERGY TO THE VIBRATION OF THE MATERIAL AS A WHOLE). THIS LIGHT OUTPUT IS CALLED SCINTILLATION. AN IMPORTANT CLASS OF DETECTORS COLLECTS THIS LIGHT AS THE SIGNAL DUE TO THE PASSAGE OF AN ELEMENTARY CHARGED PARTICLE.

THE CONVERSION OF THE COLLECTED LIGHT INTO AN ELECTRICAL SIGNAL IS DONE IN A 'PHOTOMULTIPLIER' TUBE, A KIND OF VACUUM TUBE DIODE. LIGHT ENTERS THRU A GLASS WINDOW AND STRIKES A MATERIAL, SUCH AS ANTIMONY-CESIUM, WHICH HAS A STRONG PHOTO-ELECTRIC EFFECT. (20% PROBABILITY OF EJECTING AN ELECTRON INTO THE VACUUM TUBE). THE PHOTO-ELECTRONS ARE PULLED BY AN ELECTRIC FIELD ONTO A DYNODE (ALSO OF Sb-Cs, OR Be-Cu) WHERE SECONDARY EMISSION OCCURS. TYPICALLY 3-4 SECONDARY ELECTRONS ARE EMITTED FOR EACH ELECTRON INCIDENT ON A DYNODE. A TUBE WITH 10 STAGES ACHIEVES A GAIN OF 10^5.

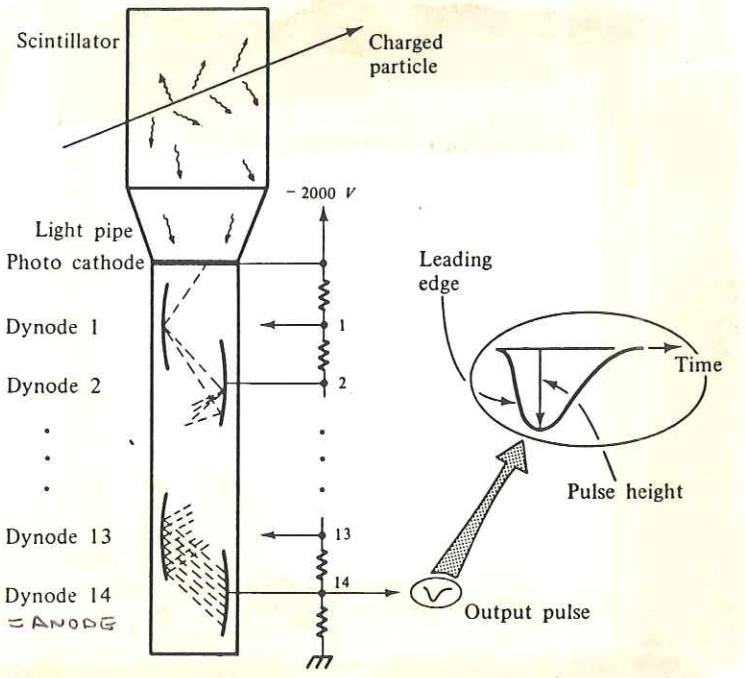

Fig. 4.2. Scintillation counter. A particle passing through the scintillator produces light which is transmitted through a light pipe onto a photomultiplier.

So for an initial signal of only 10 photoelectrons, there are 10^6 electrons collected at the anode. In a fast scintillation process all these electrons will arrive within a 10ns wide pulse, which can drive a 50mV signal into a 50Ω transmission line. Such signals readily trigger modern semi-conductor electronics such as a 10116 line receiver ⇒ bells, whistles, tape recordings etc.

The scintillation process is a bit more complicated than indicated above. If an atom has a good chance of de-exciting via photon emission, then similar neighboring atoms will readily absorb this light, possibly re-emitting it later. But as this cycle of emission and absorption is not 100% efficient, the light never reaches the surface of the material. Even most 'transparent' materials are not transparent to their own scintillation!

A typical trick is to dope the material with some other atoms or molecules which are readily excited by the scintillation light, but de-excite via a cascade of lower energy photons (longer wavelength). The host material may then be transparent to the 'wave-shifted' photons.

There are 2 broad classes of scintillators: inorganic and organic. The inorganic scintillators were first used in 1903 (Crookes) in the form of Zn-S (now used mainly on oscilloscope screens). Recent important inorganic scintillators include NaI (Th) (developed by Hofstadter at Princeton in 1947), $Bi_4Ge_3O_{12}$, and BaF. These materials have relatively high scintillation efficiency, but characteristic de-excitation times of 100-200 ns. They are high Z, high density materials and make excellent high energy photon detectors, via the electromagnetic cascade process discussed below. NaI yields about 1 scintillation photon for each 25 eV of energy deposited by a high energy particle.

Organic scintillators are mostly based on benzene ring compounds — the flatter the ring the better the scintillation. One of the very best organic scintillators is anthracene →

Most practical organic scintillators are made from toluene compounds dissolved in a suitable plastic. Organic scintillators are 4-10 times less efficient than NaI, but have very rapid de-excitation times of 1-5 ns. As such they are among the fastest of all particle detectors presently available. Scintillation detectors are often used to provide a 'trigger' signal indicating when it is appropriate to sample a slower detector.

A good organic scintillation detector can yield about 200 photo-electrons for a 1cm thickness, taking into account ~10% efficiency of light collection, and 20% photo electric efficiency. A typical scintillation counter costs $300.

Ph 529 Lecture 4

Ionization Detectors

A large class of detectors is based on collection of charges which are ionized by the passage of a high energy particle thru a gas (or even liquids and solids nowadays). It is favorable to use a gas such as argon which has a low probability of 'attaching' the ionized electrons to neutral atoms (due to possible polar nature of the atoms or molecule, or formation of meta-stable molecular states...)

An ionization detector is basically a capacitor.

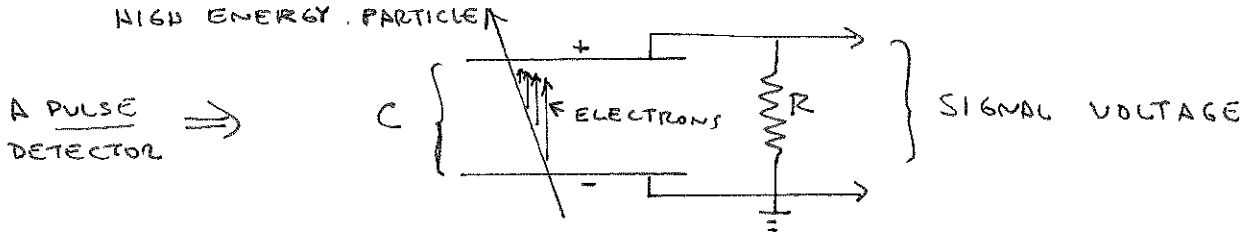

Under the influence of an applied voltage (not shown) the ionization electrons drift towards the anode plate (or wire) at typical velocity of 1 cm per micro second. (The positive ions drift in much more slowly and are ignored if the RC time constant << positive ion drift time.) With the resistor to discharge the capacitor as shown, a voltage pulse is observed with characteristic fall time RC. This is made longer than the relevant electron drift time (rise time) so as to observe maximum signal, but otherwise as short as possible.

A parallel plate ionization chamber as sketched above is not useful for detecting single minimum ionizing particles; too little charge is liberated.

Example: 1 cm of argon gas. $\rho \approx .00125$ gm/cm^2

$dE/dx|_{MIN} = 1.5$ MeV/gm/cm^2 (see table appended)

$\therefore$ energy deposition ≈ 2 KeV.

It takes ≈ 35 eV to liberate one electron $\Rightarrow$ 60 electrons/cm

This is too few for even the best low noise, high speed amplifiers to detect.

Parallel plate ion chambers find application in monitoring intensities of beams of 10^6 or more high energy particles, or in observation of low energy nuclear reactions in which recoiling nuclei may yield 10^6 times minimum ionization...

AN IMPORTANT VARIATION, DUE TO RUTHERFORD & GEIGER (1908) UTILIZES CYLINDRICAL GEOMETRY. AS ELECTRONS DRIFT TOWARDS THE ANODE WIRE THEY FIND THEMSELVES IN STRONGER AND STRONGER ELECTRIC FIELDS. IF THE POTENTIAL DIFFERENCE IN ONE MEAN FREE PATH OF THE DRIFTING ELECTRON IS GREATER THAN THE IONIZATION POTENTIAL OF THE GAS, THEN 'GAS AMPLIFICATION' OCCURS.

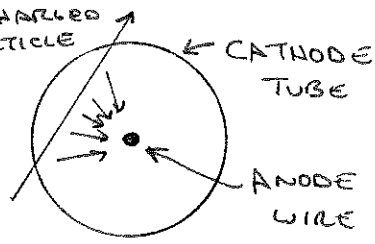

SECONDARY IONIZATION TAKES PLACE DURING ELECTRON - ATOM COLLISIONS — LEADING TO A CHAIN REACTION. MOST OF THE SECONDARY IONIZATION OCCURS VERY CLOSE TO THE ANODE WIRE, SO THE RISE TIME OF THE PULSE CAN BE QUITE SHORT ~ 20 NS.

AN IMPORTANT CONTRIBUTION TO THE CHAIN REACTION PROCESS COMES FROM ULTRAVIOLET PHOTONS LIBERATED DURING RECOMBINATION OF IONIZED ATOMS. THESE CAN TRAVEL AT RIGHT ANGLES TO THE ELECTRIC FIELD LINES, AND PROPAGATE THE CHAIN REACTION ALONG THE ENTIRE ANODE WIRE — LEADING TO THE GEIGER DISCHARGE. THIS GIVES A VERY LARGE SIGNAL, READILY DETECTED WITH 1908 ELECTRONICS. HOWEVER THE CHAMBER IS RENDERED USELESS FOR QUITE SOME TIME AFTER SUCH A DISCHARGE. NOWADAYS ELECTRONIC AMPLIFIERS ARE SENSITIVE ENOUGH THAT THERE IS LITTLE NEED FOR THE U-V PHOTON CONTRIBUTION TO THE GAS AMPLIFICATION PROCESS. TYPICALLY CERTAIN GASES ARE ADDED IN SMALL AMOUNTS TO 'QUENCH' THE U.V. PROPAGATION. A USEFUL DISCHARGE OF GAS AMPLIFICATION FACTOR ~ 10^4 CAN BE HELD TO ONLY 50–100 NS.

EXAMPLE: A TUBE OF RADIUS 1 cm FILLED WITH ARGON.

A MINIMUM IONIZING PARTICLE WITH 1 cm PATH THEN LEADS TO A DISCHARGE OF 6×10^5 ELECTRONS, IN SAY A 50 NS PULSE. THIS LEADS TO A 200 μV SIGNAL INTO 100 Ω. (IF RC CONSTANT SHORT ENOUGH)

WELL DESIGNED INTEGRATED CIRCUIT AMPLIFIERS CAN PROCESS THIS SIGNAL FURTHER.

A COMMON IMPLEMENTATION OF THE CYLINDRICAL GEOMETRY IS THE MULTI-WIRE PROPORTIONAL CHAMBER (MWPC). IN THESE, THERE ARE 2 PLANES OF CATHODE WIRES SURROUNDING A PLANE OF ANODE WIRES

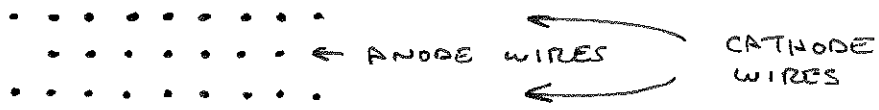

EACH ANODE WIRE IS APPROXIMATELY IN A CYLINDRICAL ENVIRONMENT.

TYPICAL WIRE SPACING IS 1-2 MM, WHILE THE ANODE WIRES ARE USUALLY .0008" DIAMETER. SUCH A DEVICE GIVES .3 MM POSITION RESOLUTION (IF 1 MM WIRE SPACING) OVER AREAS OF 1-2 M^2. THE COST IS ABOUT $30 A WIRE.

ANOTHER VARIATION IS THE DRIFT CHAMBER. HERE ONE ANODE WIRE IS PLACED WITHIN AN ELONGATED CELL OF CATHODE WIRES HELD AT GRADED POTENTIALS

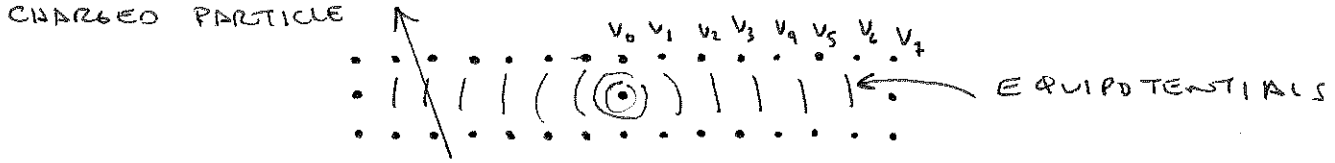

THE GRADING CREATES A UNIFORM ELECTRIC FIELD OVER MOST OF THE CELL, BUT NEAR THE ANODE WITH A CYLINDRICAL GEOMETRY OBTAINS. THUS THE IONIZATION ELECTRONS DRIFT AT UNIFORM VELOCITY OVER MOST OF THE CELL BEFORE INITIATING GAS AMPLIFICATION CLOSE TO THE ANODE WIRE. BY MEASURING THE DRIFT TIME (RELATIVE TO A START SIGNAL SUPPLIED BY A SCINTILLATION COUNTER) THE POSITION OF THE PRIMARY IONIZATION CAN BE DETERMINED TO AN ACCURACY OF .1 - .2 MM. DRIFT DISTANCES OF UP TO 10 CM HAVE BEEN ACHIEVED. MANY FEWER WIRES ARE REQUIRED IN A DRIFT-CHAMBER THAN IN A MWPC, BUT THE COST OF THE TIME MEASURING ELECTRONICS IS HIGHER (~ $200/WIRE).

COHERENT RADIATION DETECTORS

AN INTERESTING TYPE OF PARTICLE DETECTOR INVOLVES THE COHERENT RESPONSE OF A MATERIAL TO THE PASSAGE OF A HIGH ENERGY CHARGED PARTICLE. EXAMPLES ARE THE ČERENKOV COUNTER AND THE TRANSITION RADIATION DETECTOR

THE ČERENKOV EFFECT OCCURS WHEN THE MOVING PARTICLE HAS VELOCITY GREATER THAN THE GROUP VELOCITY OF LIGHT IN THE MATERIAL; I.E. $v > c/n$ WHERE n = INDEX OF REFRACTION. THEN THE COHERENT ACTION OF THE MATERIAL WHICH NORMALLY PRODUCES WAVES THAT TRAVEL WITH VELOCITY c/n CAN NOT KEEP UP WITH THE PARTICLE, LEADING TO A 'SHOCK WAVE' RESPONSE.

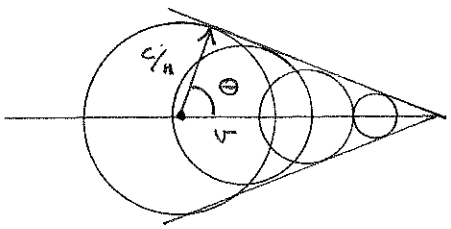

$$\cos\theta = \frac{c}{nv} = \frac{1}{n\beta}$$

THE INTENSITY OF THE RADIATION IS QUITE LOW, BEING ABOUT $500 \sin^2\theta$ PHOTONS/CM IN THE VISIBLE LIGHT SPECTRUM.

THE ČERENKOV EFFECT CAN BE UTILIZED IN A THRESHOLD DETECTOR, WHICH RESPONDS TO ALL PARTICLES OF VELOCITY $v > c/n$

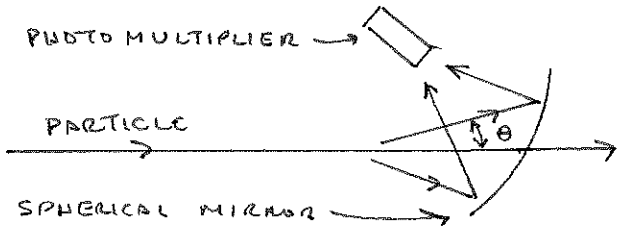

OPTICS EXERCISE: SHOW THAT A LINE SOURCE OF LIGHT WHICH PRODUCES CONES OF RAYS OF ANGLE θ, IS FOCUSSED TO A RING IMAGE BY A SPHERICAL MIRROR!

THE INDEX n OF A GAS CAN BE TUNED BY VARYING ITS DENSITY

$$n^2 = 1 + \frac{4\pi N e^2}{m_e \omega^2}$$

N = NUMBER DENSITY OF ATOMIC ELECTRONS

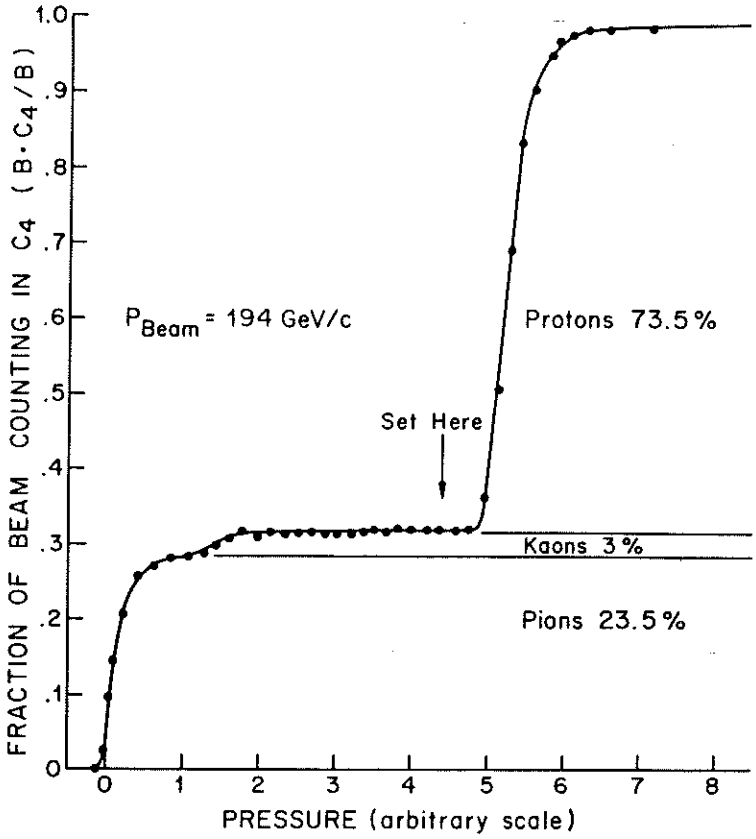

FIGURE 2-5. PRESSURE CURVE FOR C_4. AS THE HELIUM PRESSURE IN THE BEAM PIPE IS INCREASED, THE INDEX OF REFRACTION IS INCREASED AND HEAVIER PARTICLES BEGIN TO CAUSE CERENKOV RADIATION. AS SEEN IN THE FIGURE, A VERY GOOD SEPARATION OF PIONS AND PROTONS WAS POSSIBLE. KAONS WERE COUNTED AS PIONS UNDER NORMAL RUNNING CONDITIONS.

A BEAM OF PARTICLES PREPARED WITH THE AID OF VARIOUS MAGNETS MIGHT CONTAIN PARTICLES OF SEVERAL DIFFERENT MASSES, BUT ALL OF THE SAME MOMENTUM p. THEN VELOCITY $v = p/m$ DEPENDS ON THE PARTICLE TYPE. IF THERE ARE M PARTICLE TYPES, THEY COULD BE IDENTIFIED BY TYPE WITH THE USE OF $M-1$ THRESHOLD ČERENKOV COUNTERS — IN A NON-DESTRUCTIVE WAY.

DIFFERENTIAL ČERENKOV COUNTERS USE VARIOUS OPTICAL BAFFLES SO AS TO COLLECT LIGHT EMITTED ONLY IN A SMALL ANGULAR RANGE $\Delta\theta$ WITH RESPECT TO THE PARTICLE'S DIRECTION. THEN A SINGLE SUCH DEVICE CAN IDENTIFY EXACTLY 1 PARTICLE TYPE IN A MIXED BEAM OF KNOWN MOMENTUM. THIS WORKS WELL ONLY IN WELL COLLIMATED BEAMS SO THAT $\Delta\theta$ IS SHARPLY DEFINED.

TRANSITION RADIATION DETECTORS UTILIZE THE CHANGE IN SHAPE OF THE ELECTRIC FIELD ACROSS THE BOUNDARY BETWEEN 2 DIELECTRIC MEDIA. THE FIELD OF A MOVING CHARGE IS CONTINUALLY REARRANGING ITSELF AT THE BOUNDARY, RESULTING IN A PULSE OF RADIATION IN ADDITION TO THE 'STATIC' FIELD COMPONENT. THIS EFFECT IS MUCH WEAKER THAN ČERENKOV RADIATION, BUT THE INTENSITY VARIES AS γ^4 WHERE $\gamma = 1/\sqrt{1 - v^2/c^2}$

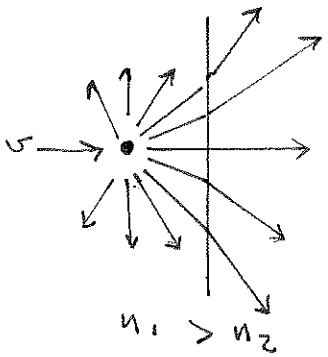

TRANSITION RADIATION DETECTORS FIND THEIR MAIN APPLICATION IN THE IDENTIFICATION OF ELECTRONS NON-DESTRUCTIVELY (AS THEY HAVE THE HIGHEST γ FOR A GIVEN ENERGY). THE TRANSITION RADIATION IS MAINLY IN X-RAY FREQUENCIES, REQUIRING INTERESTING TECHNOLOGY FOR ITS OBSERVATION.

[AVAILABLE ON REQUEST ARE A SET OF NOTES DERIVING THE INTENSITY AND SPECTRUM OF γ TRANSITION RADIATION - WITHOUT USE OF BESSEL FUNCTIONS.]

WE NOW CONSIDER A CLASS OF DETECTORS OF ELECTRONS, PHOTONS AND CHARGED OR NEUTRAL HADRONS WHICH DEPEND ON THE ENERGETIC PARTICLE INITIATING A 'SHOWER' OF HIGH ENERGY INTERACTIONS. FIRST WE GIVE SOME DETAILS OF HIGH ENERGY ELECTRON AND PHOTON INTERACTIONS WITH MATTER.

INTERACTIONS OF ELECTRONS WITH MATTER - BREMSSTRAHLUNG

AS ELECTRONS PASS THRU MATTER THEY SUFFER dE/dx LOSSES AND MULTIPLE COULOMB SCATTERING AS DO HEAVIER PARTICLES. HOWEVER, RELATIVISTIC ELECTRONS ARE EVEN MORE STRONGLY AFFECTED BY BREMSSTRAHLUNG = RADIATION OF PHOTONS DURING COULOMB COLLISIONS WITH THE NUCLEUS. THE RADIATION RATE DEPENDS ON THE SQUARE OF THE ACCELERATION $\sim (F/M)^2$. ONLY FOR THE RELATIVELY LIGHT ELECTRONS IS BREMSSTRAHLUNG A SIGNIFICANT LOSS MECHANISM.

WE GIVE A SEMI-CLASSICAL ARGUMENT. RECALL THE LARMOR FORMULA FOR RADIATION BY AN ACCELERATED CHARGE AT LOW VELOCITIES $v \ll c$.

$$\frac{dU}{dt} = \frac{2}{3}\frac{e^2 a^2}{c^3}$$. WE NEED THE RESULT AS $v \to c$, AND $\bar{a} \perp \bar{v}$ AS IN A COULOMB COLLISION.

A KEY FACT IS THAT dU/dt IS A RELATIVISTIC INVARIANT: ENERGY U AND TIME t BOTH TRANSFORM AS THE TIME COMPONENT OF A 4-VECTOR.

THUS $$\left.\frac{dU}{dt}\right|_{LAB} = \frac{2}{3}\frac{e^2}{c^3}\, a^2_{\text{ELECTRONS REST FRAME}}$$

IN THE ELECTRON'S REST FRAME THE NUCLEUS MOVES WITH VELOCITY $-\bar{v}$, SO ITS FIELD STRENGTH IS BOOSTED TO $\gamma Ze/b^2$, AT IMPACT PARAMETER b.

HENCE $a \to \frac{\gamma Z e^2}{b^2 m_e}$ AND $$\left.\frac{dU}{dt}\right|_{LAB} = \frac{2}{3}\frac{\gamma^2 Z^2 e}{b^4 m_e^2 c^3}$$

THE PULSE OF RADIATION LASTS TIME $\Delta t \sim 2b/c$ IN THE LAB, SO

$$U = \frac{4}{3}\frac{\gamma^2 Z^2 e^2}{b^3}\left(\frac{e^2}{m_e c^2}\right)^2$$

The lab frequency spectrum is the Lorentz transform of the rest frame spectrum. In the rest frame the pulse lasts time

$$\Delta t^* \approx \frac{b}{\gamma c}$$

due to the Lorentz contraction of the field of the nucleus. Such a pulse has a flat frequency spectrum up to

$$\nu^*_{MAX} = \frac{1}{\Delta t^*} \sim \gamma c/b$$

On transforming this spectrum to the lab, the maximum frequency is $\nu_{MAX} \sim \gamma \nu^*_{MAX} \sim \gamma^2 c/b$

Again a pulse leads to a flat energy spectrum

$$\frac{dU}{d\nu} = \frac{U_{TOTAL}}{\nu_{MAX}} = \frac{4}{3}\frac{Z^2 e^2}{b^2 c}\left(\frac{e^2}{m_e c^2}\right)^2$$

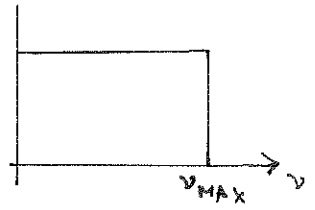

We may convert the energy spectrum to a photon number spectrum by dividing by $h\nu$: $dN = dU/h\nu$

so $$\frac{dN}{d h\nu} = \frac{2}{3\pi}\frac{Z^2}{b^2}\left(\frac{e^2}{\hbar c}\right)\left(\frac{e^2}{m_e c^2}\right)^2 \frac{1}{h\nu}$$

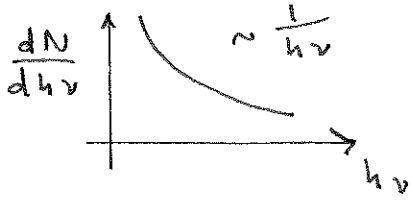

Note the characteristic $1/E_\gamma$ fall off of the bremsstrahlung spectrum.

We can now estimate the radiation loss by an electron in crossing a slab of material of thickness dx (gm/cm^2)

$$dE = \frac{N_0}{A}\, dx \int_{b_{MIN}}^{b_{MAX}} 2\pi b\, db\, U_{TOTAL}(b)$$

In the relativistic limit we cannot immediately use our result $U_{TOTAL} = \frac{\gamma^2 Z^2 e^2}{b^3}\left(\frac{e^2}{m_e c^2}\right)^2$. Instead we must note that the maximum energy photon possible is just the energy of the electron itself. Thus $h\nu_{MAX} = E$. The subtlety is that the energy spectrum remains as derived above, only it is cut off at lower ν_{MAX}.

Our revised estimate is then $U(b) = \frac{dU}{d\nu}\cdot\frac{E}{h} = \frac{2}{3\pi}\frac{Z^2}{b^2}\left(\frac{e^2}{\hbar c}\right)\left(\frac{e^2}{m_e c^2}\right)^2 \cdot E$

and $$\frac{1}{E}\frac{dE}{dx} = \frac{2}{3\pi}\frac{N_0}{A} Z^2 \alpha r_e^2 \int 2\pi b\, \frac{db}{b^2} = \frac{4}{3}\alpha\frac{N_0}{A} Z^2 r_e^2 \ln\left(\frac{b_{MAX}}{b_{MIN}}\right)$$

Again $b_{MAX} \sim$ radius of atom $\sim \frac{r_e}{\alpha^2 Z^{1/3}}$

[Note that so long as $\gamma > 137$, $h\nu_{MAX} \sim \frac{h\gamma^2 c}{b_{MAX}} > E_{ELECTRON}$]

while b_{MIN} can be thought of as $\frac{\hbar}{m_e c} = \frac{r_e}{\alpha} \equiv$ electron Compton wavelength (a bit of a swindle)

IF WE ACCEPT THE ABOVE ESTIMATES, WE FIND

$$\frac{1}{E}\frac{dE}{dx} = \frac{4}{3} \alpha \frac{N_0}{A} Z^2 r_e^2 \ln\left(\frac{137}{Z^{1/3}}\right)$$

A DETAILED CALCULATION, BETHE-HEITLER (1934), SHOWS

$$\frac{1}{E}\frac{dE}{dx} = 4 \alpha \frac{N_0}{A} Z^2 r_e^2 \left[\ln\left(\frac{183}{Z^{1/3}}\right) + \frac{1}{18}\right]$$

THEY INTRODUCED THE DEFINITION OF THE RADIATION LENGTH $\equiv X_0$ ON THIS BASIS:

$$\frac{1}{E}\frac{dE}{dx} = \frac{1}{X_0} \quad \longleftrightarrow \quad E = E_0 e^{-x/X_0}$$

ELECTRONS OF ALL ENERGIES (ONCE γ LARGE) RADIATE AWAY $\sim 2/3$ OF THEIR ENERGY IN ONE RADIATION LENGTH!

AS FAR AS INTERACTIONS WITH MATTER ARE CONCERNED, A HIGH ENERGY ELECTRON IS ONE FOR WHICH THE RADIATION LOSS IS GREATER THAN THE IONIZATION LOSS TO ATOMS. THIS CRITICAL ENERGY IS ABOUT

$$E_c \sim \frac{3\pi}{2 r_e} \sim \frac{600\,\text{MeV}}{Z}$$

COMPARING WITH P. 42.

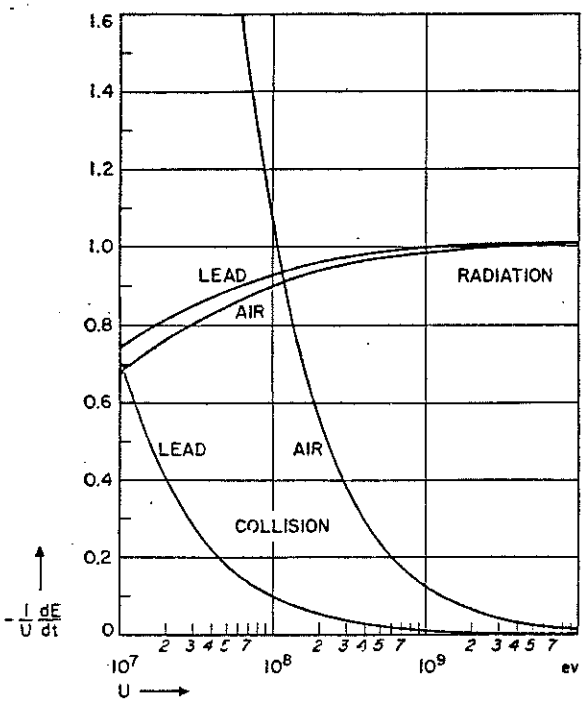

Fig. 2.11.4. Fractional energy loss by collision, $-\frac{1}{U}\left(\frac{dE}{dt}\right)_{col}$, and fractional energy loss by radiation, $-\frac{1}{U}\left(\frac{dE}{dt}\right)_{rad}$, for electrons, per radiation length of *air* or *lead*.

THAT IS, THE "CRITICAL ENERGY" IS THE ENERGY LOSS TO IONIZATION WHEN A PARTICLE TRAVERSES ONE RADIATION LENGTH.

ABSORPTION OF PHOTONS DUE TO PAIR PRODUCTION

LOW ENERGY INTERACTIONS OF PHOTONS WITH MATTER ARE DOMINATED BY COMPTON SCATTERING (= THOMSON SCATTERING AT VERY LOW ENERGIES), AND BY THE PHOTO-ELECTRIC EFFECT. BUT IF $E_\gamma > 2 m_e c^2$, THE PHOTON CAN VANISH, PRODUCING AN e^+e^- PAIR.

THE BETHE-HEITLER PROCESS WAS MENTIONED IN LECTURE 3, AND IT WAS INDICATED THAT DIMENSIONAL ARGUMENTS LEAD TO A CROSS SECTION ESTIMATE

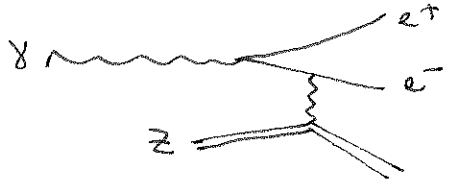

$$\sigma \sim \frac{Z^2 \alpha^3}{m_e^2} \ln \frac{E_\gamma}{m_e} \sim \alpha Z^2 r_e^2 \ln \frac{E_\gamma}{m_e}$$

[NOTE ALSO THAT THE ENERGY SPECTRUM OF THE e^+ OR e^- IS ESSENTIALLY FLAT BETWEEN 0 AND E_γ]

THE DETAILED WORK OF BETHE & HEITLER SHOWED THAT THE PAIR PRODUCTION RATE PER gm/cm^2 TRAVERSED IS

$$\frac{7}{9} \underbrace{4 \kappa \frac{N_0}{A} Z^2 r_e^2 \ln \frac{183}{Z^{1/3}}}_{1/X_0} \qquad \text{(FOR } E_\gamma \gg 300 \text{ MeV)}$$

THUS HIGH ENERGY PHOTONS PRODUCE A PAIR TYPICALLY BEFORE TRAVERSING ONE RADIATION LENGTH.

$$N_\gamma = N_0 e^{-\frac{7}{9}\frac{x}{X_0}}$$

AGAIN, THE PAIR PRODUCTION MECHANISM BECOMES MORE IMPORTANT THAN COMPTON SCATTERING AT ABOUT THE CRITICAL ENERGY DEFINED ON P 54.

NOTE HOWEVER THE SLOW RISE IN THE PAIR PRODUCTION RATE UNTIL THE ASYMPTOTIC VALUE IS ACHIEVED AT ABOUT 1 GeV. (BELOW 1 GeV THE TERM $\ln E_\gamma/m_e$ IS STILL IMPORTANT)

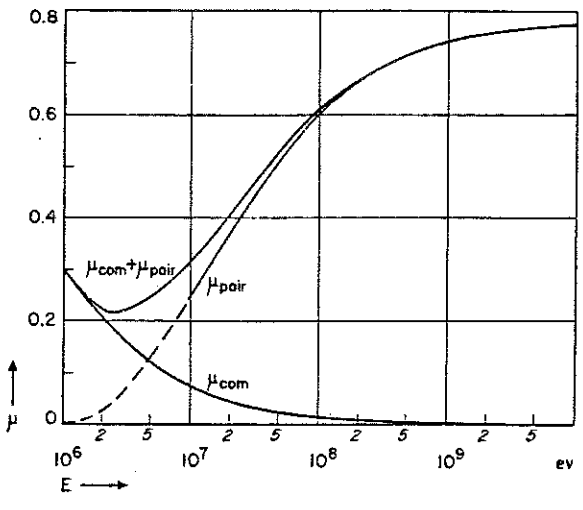

Fig. 2.19.4. The total probability for radiation length of *lead* for Compton scattering (μ_{com}), for pair production (μ_{pair}) and for either effect ($\mu_{com} + \mu_{pair}$). For $E < 10^7$ ev, μ_{pair} cannot be calculated with the text and a more accurate equation must be used (BHA34). From Rossi and Greisen (RB41.1).

WE NOTE THAT CHARGED PARTICLES CAN ALSO PRODUCE ELECTRON-POSITRON PAIRS BY DIAGRAMS AS SKETCHED. THIS PROCESS, AND BREMSSTRAHLUNG ARE QUITE RARE FOR HEAVY PARTICLES, BUT CAN LEAD TO VERY LARGE ENERGY LOSSES IN A SINGLE COULOMB COLLISION. MOST OF THE LARGE FLUCTUATIONS IN DEPOSITED ENERGY ARE DUE TO THESE PROCESSES.

Ph 529 Lecture 4

Electromagnetic Showers

When high energy electrons or photons enter a block of material they do not deposit their energy all at once. Rather they initiate a cascade of secondary electrons and photons. Each electron radiates photons, and photons produce more electrons via pair production, until the energies drop below the critical energy. (What happens then?)

If the initial electron or photon energy is E, we might then expect E/E_c electrons in the entire cascade (counting each electron anew after one radiation length). The number of generations in the shower is then

$$2^N = E/E_c \quad \text{or} \quad N = \frac{\ln(E/E_c)}{\ln 2}$$

Each generation of radiation + pair production penetrates about 2 additional radiation lengths into the material.

Example: $E < 100$ GeV, material = lead, with $E_c = 7$ MeV

Then $N \sim 14 \Rightarrow 28$ radiation lengths of shower.

Indeed to contain 99% of the energy of a 100 GeV shower takes over 20 X_0 in practice.

As the shower develops some of the electrons and photons move transversely to the initial direction. But the entire cascade is reasonably well contained within a radius of $1\,X_0$ for heavy materials.

A better approximation for the shower radius is

$$r_{\text{shower}} \sim 1 X_0 \cdot \frac{21}{E_c \text{ in MeV}}$$

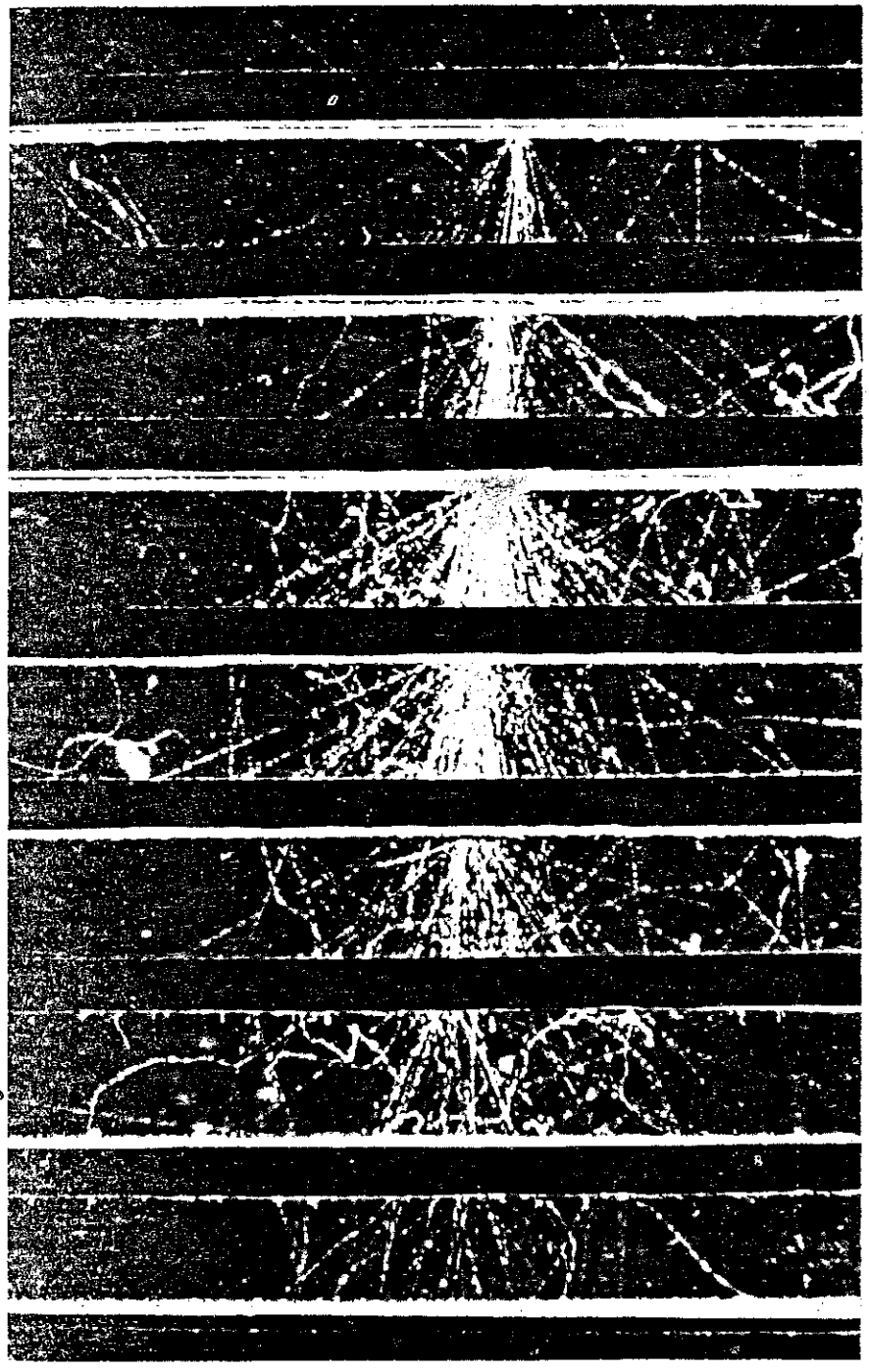

Fig. 5.1.1. Cloud-chamber picture of a large cascade shower. The plates across the chamber are lead, 1.27 cm thick. From C. Y. Chao.

$L \sim 2$ radiation lengths

Ph 529 Lecture 4

Strong Interactions of Hadrons with Matter

Particles containing quarks (=hadrons) occasionally interact strongly with nuclei as they traverse a block of material. These interactions are rare but violent, and determine the large scale features of the penetration of hadrons in matter.

The cross section for inelastic scattering of a high energy hadron on a nucleus of atomic number A is about $40\,\text{mb} \cdot A^{2/3} \cdot$ # of quarks in hadron (Why $A^{2/3}$?)

By 'inelastic' we mean a reaction in which the final state includes other particles than the original hadron and nucleus. This can happen 2 ways: additional hadrons, mostly π mesons, are produced; and the nucleus may break up into various fragments. The passage of hadrons thru matter is little affected by elastic nuclear scattering which gives little net contribution to energy loss, and whose cross-section is only $\sim 5\,\text{mb} \cdot A^{2/3}$.

The inelastic cross section is quite small, so the high energy hadron has a fairly long mean free path. Values of this mean free path ≡ nuclear interaction length are listed for protons in the table appended to this lecture. (Can you verify these values starting from the cross section given above?). A representative value is the interaction length in solid iron of 7 inches.

The interaction length for neutrons is essentially the same as for protons. After its first inelastic nuclear interaction a neutron can be 'observed' via the secondary charged particles. The interaction length for π & K mesons is about 3/2 that for protons, as their cross sections are only 2/3 as large.

In an inelastic collision the number of secondary hadrons produced is a slow function of the interaction energy. The secondaries are mainly π mesons, π^+, π^0, π^-, so that charged secondaries out number neutrals by about 2 to 1. The π^0 mesons decay quickly ($\sim 10^{-16}$ sec) via $\pi^0 \to \gamma\gamma$, which causes electromagnetic showers. For materials of atomic number greater than carbon, the radiation length is smaller than the interaction length, so the latter sets the scale of the hadronic cascade process.

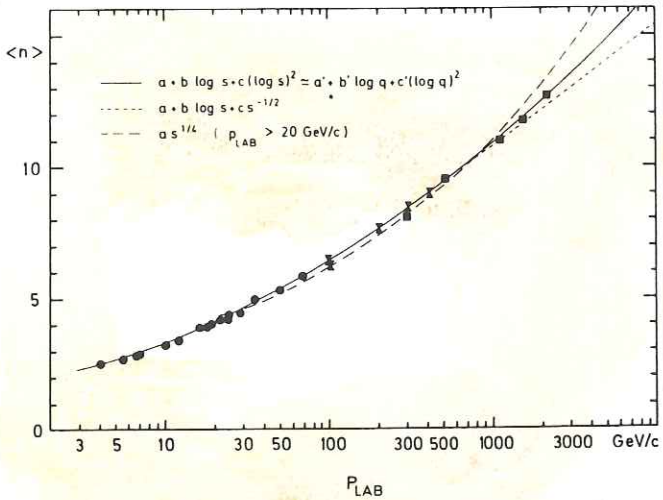

Mean-value of the total charged multiplicity as a function of p_{lab}.

THE ENERGY OF THE SECONDARY PARTICLES HAS A BREMSSTRAHLUNG-LIKE DISTRIBUTION: $P(E)\,dE \sim dE/E$. THE HIGHEST-ENERGY SECONDARY HAS ENERGY $E/2$ ON AVERAGE.

THE SECONDARY PARTICLES TRAVEL THRU THE MATERIAL, LOSING ENERGY SLOWLY BY IONIZATION UNTIL THEY SUFFER STRONG NUCLEAR INTERACTIONS. IN EACH NUCLEAR INTERACTION ABOUT 200 MeV IS LOST TO NUCLEAR BINDING ENERGY, AND IN IRON ABOUT 300 MeV IS LOST TO IONIZATION BETWEEN EACH NUCLEAR INTERACTION. THUS THE TOTAL NUMBER OF NUCLEAR INTERACTIONS INDUCED BY A HADRON OF ENERGY E IS $N \sim E/500\ \text{MeV}$, AND THE NUMBER OF GENERATIONS IS $n = \ln N/\ln 2$.

FOR EXAMPLE, A 100-GeV PROTON WILL TYPICALLY PRODUCE A SHOWER OF 8 PION INTERACTION LENGTHS ($= 3/2$ PROTON INT. LENGTHS) $\Rightarrow \sim 2$ METERS LONG.

A HADRON CALORIMETER IS A DEVICE TO MEASURE THE TOTAL ENERGY DEPOSITED IN THE SHOWER DESCRIBED ABOVE. BECAUSE OF THE GREAT MASS OF MATERIAL REQUIRED TO CONTAIN A HADRONIC SHOWER, CALORIMETERS ARE ALMOST ALWAYS MULTILAYER SANDWICHES OF A DENSE MATERIAL SUCH AS IRON, AND PARTICLE DETECTORS SUCH AS SCINTILLATORS OR MWPC'S. SEVERAL SAMPLES OF THE PARTICLE TRACKS ARE TAKEN EACH INTERACTION LENGTH. GOOD PERFORMANCE IS ACHIEVED ONLY IF THERE IS ABOUT 1 SAMPLE PER RADIATION LENGTH TO COLLECT THE π^0 PART OF THE SHOWER. IN EFFECT, ONE TRIES TO DETERMINE THE TOTAL PATH LENGTH TRAVELLED BY CHARGED PARTICLES, AND THEN USE THE MINIMUM-IONIZATION ENERGY LOSS OF $\sim 1.5\ \text{MeV}/(\text{gm}/\text{cm}^2)$ TO ESTIMATE THE TOTAL ENERGY.

A SERIOUS DIFFICULTY IS THAT THE ENERGY SPENT IN NUCLEAR BREAKUP (~ 200 MeV/INTERACTION) IS POORLY SAMPLED BY THIS TECHNIQUE. STATISTICAL FLUCTUATIONS IN THIS UNSAMPLED ENERGY, 40% OF THE TOTAL ON AVERAGE LIMIT THE ENERGY RESOLUTION:

$N = E/500\ \text{MeV}$ NUCLEAR INTERACTIONS $\Rightarrow \sqrt{N}$ FLUCTUATION

$$\text{i.e.}\quad \frac{\sigma_E}{E} = \frac{1}{\sqrt{N}} = \frac{1}{\sqrt{2E_{\text{in GeV}}}} \sim \frac{70\%}{\sqrt{E_{\text{in GeV}}}} \quad \text{IN IRON.}$$

THE USE OF URANIUM RATHER THAN IRON LEADS TO SOMEWHAT SMALLER LOSSES DUE TO NUCLEAR BREAKUP AND RESOLUTIONS OF $50\%/\sqrt{E}$ ARE REPORTED.

DESPITE THIS POOR RESOLUTION, HADRON CALORIMETERS ARE BECOMING INCREASINGLY IMPORTANT IN VERY HIGH ENERGY EXPERIMENTS WHERE KNOWLEDGE OF THE TOTAL ENERGY BALANCE IS IMPORTANT. FOR EXAMPLE, THE DISCOVERY OF THE W BOSON VIA THE DECAY $W \to e\nu$ DEPENDED ON SHOWING THAT THE NEUTRINO ESCAPED DETECTION WHILE CARRYING AWAY ENERGY $\sim M_W/2 \sim 40$ GeV.

A LARGE MULTIPARTICLE DETECTOR

ON THE NEXT PAGE IS SKETCHED THE DETECTOR OF THE LEP-3 GROUP WHICH OPERATES AT CERN TO OBSERVE $e^+e^- \to Z^0$ AND THE SUBSEQUENT DECAY OF THE Z^0. IT EMPHASIZES CALORIMETRY OF ELECTRONS, PHOTONS AND HADRONS, AND MAGNETIC MEASUREMENT OF MUONS. THE DETECTOR IS QUITE LARGE.

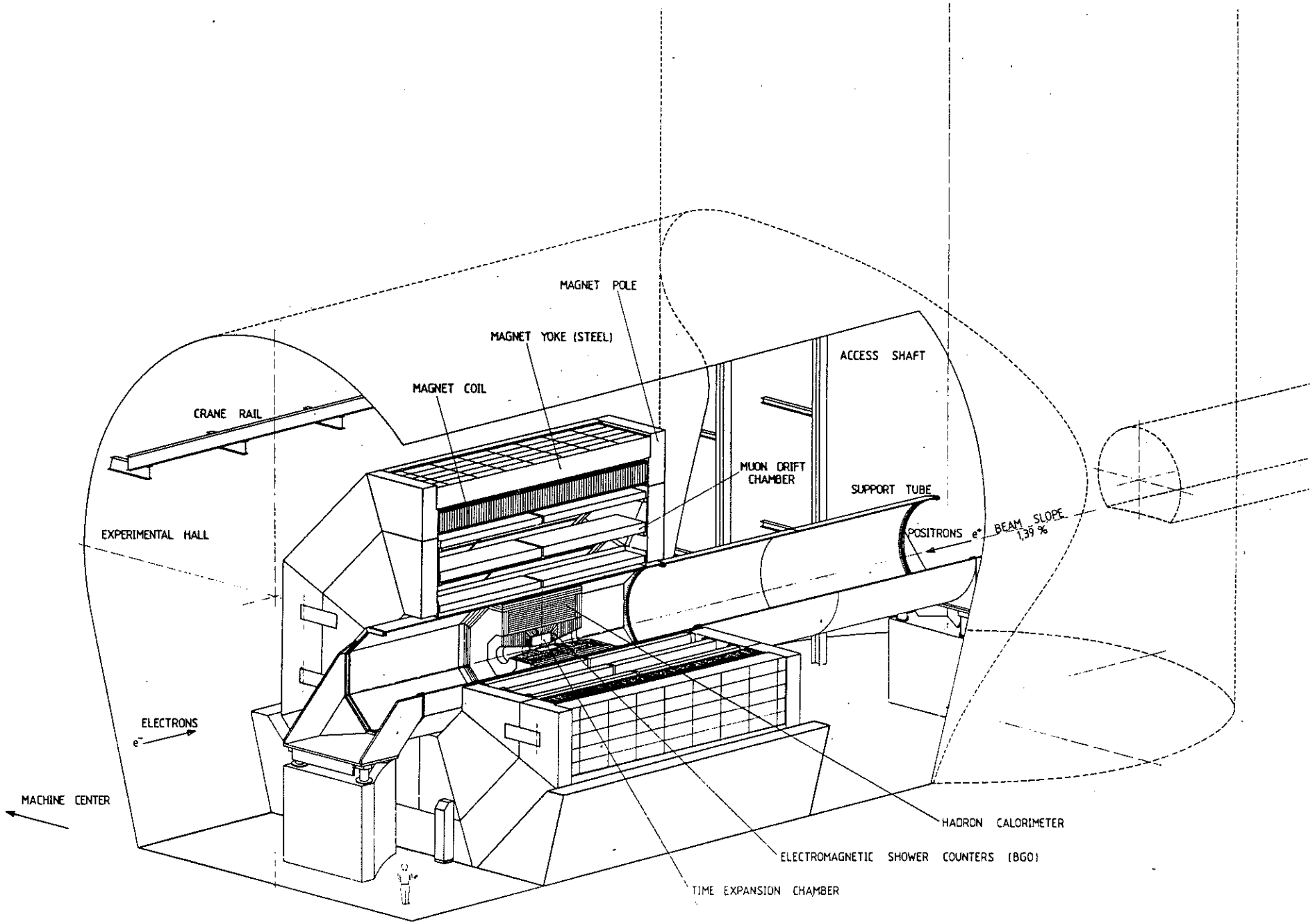

FIG.1 LEP-3 DETECTOR

6. ATOMIC AND NUCLEAR PROPERTIES OF MATERIALS

Table 6.1 Abridged from `pdg.lbl.gov/AtomicNuclearProperties` by D.E. Groom (2015). See web pages for more detail about entries in this table and for several hundred other substances. Parentheses in the dE/dx and density columns indicate gases at 20° C and 1 atm. Boiling points are at 1 atm. Refractive indices n are evaluated at the sodium D line blend (589.2 nm); values $\gg 1$ in brackets indicate $(n-1)\times 10^6$ for gases at 0° C and 1 atm.

Material	Z	A	$\langle Z/A\rangle$	Nucl.coll. length λ_T {g cm^{-2}}	Nucl.inter. length λ_I {g cm^{-2}}	Rad.len. X_0 {g cm^{-2}}	$dE/dx\|_{\rm min}$ { MeV g^{-1}cm^2}	Density {g cm^{-3}} ({gℓ^{-1}})	Melting point (K)	Boiling point (K)	Refract. index @ Na D
H_2	1	1.008(7)	0.99212	42.8	52.0	63.04	(4.103)	0.071(0.084)	13.81	20.28	1.11[132.]
D_2	1	2.01410177803(8)	0.49650	51.3	71.8	125.97	(2.053)	0.169(0.168)	18.7	23.65	1.11[138.]
He	2	4.002602(2)	0.49967	51.8	71.0	94.32	(1.937)	0.125(0.166)		4.220	1.02[35.0]
Li	3	6.94(2)	0.43221	52.2	71.3	82.78	1.639	0.534	453.6	1615.	
Be	4	9.0121831(5)	0.44384	55.3	77.8	65.19	1.595	1.848	1560.	2744.	
C diamond	6	12.0107(8)	0.49955	59.2	85.8	42.70	1.725	3.520			2.42
C graphite	6	12.0107(8)	0.49955	59.2	85.8	42.70	1.742	2.210			
N_2	7	14.007(2)	0.49976	61.1	89.7	37.99	(1.825)	0.807(1.165)	63.15	77.29	1.20[298.]
O_2	8	15.999(3)	0.50002	61.3	90.2	34.24	(1.801)	1.141(1.332)	54.36	90.20	1.22[271.]
F_2	9	18.998403163(6)	0.47372	65.0	97.4	32.93	(1.676)	1.507(1.580)	53.53	85.03	[195.]
Ne	10	20.1797(6)	0.49555	65.7	99.0	28.93	(1.724)	1.204(0.839)	24.56	27.07	1.09[67.1]
Al	13	26.9815385(7)	0.48181	69.7	107.2	24.01	1.615	2.699	933.5	2792.	
Si	14	28.0855(3)	0.49848	70.2	108.4	21.82	1.664	2.329	1687.	3538.	3.95
Cl_2	17	35.453(2)	0.47951	73.8	115.7	19.28	(1.630)	1.574(2.980)	171.6	239.1	[773.]
Ar	18	39.948(1)	0.45059	75.7	119.7	19.55	(1.519)	1.396(1.662)	83.81	87.26	1.23[281.]
Ti	22	47.867(1)	0.45961	78.8	126.2	16.16	1.477	4.540	1941.	3560.	
Fe	26	55.845(2)	0.46557	81.7	132.1	13.84	1.451	7.874	1811.	3134.	
Cu	29	63.546(3)	0.45636	84.2	137.3	12.86	1.403	8.960	1358.	2835.	
Ge	32	72.630(1)	0.44053	86.9	143.0	12.25	1.370	5.323	1211.	3106.	
Sn	50	118.710(7)	0.42119	98.2	166.7	8.82	1.263	7.310	505.1	2875.	
Xe	54	131.293(6)	0.41129	100.8	172.1	8.48	(1.255)	2.953(5.483)	161.4	165.1	1.39[701.]
W	74	183.84(1)	0.40252	110.4	191.9	6.76	1.145	19.300	3695.	5828.	
Pt	78	195.084(9)	0.39983	112.2	195.7	6.54	1.128	21.450	2042.	4098.	
Au	79	196.966569(5)	0.40108	112.5	196.3	6.46	1.134	19.320	1337.	3129.	
Pb	82	207.2(1)	0.39575	114.1	199.6	6.37	1.122	11.350	600.6	2022.	
U	92	[238.02891(3)]	0.38651	118.6	209.0	6.00	1.081	18.950	1408.	4404.	
Air (dry, 1 atm)			0.49919	61.3	90.1	36.62	(1.815)	(1.205)		78.80	[289]
Shielding concrete			0.50274	65.1	97.5	26.57	1.711	2.300			
Borosilicate glass (Pyrex)			0.49707	64.6	96.5	28.17	1.696	2.230			
Lead glass			0.42101	95.9	158.0	7.87	1.255	6.220			
Standard rock			0.50000	66.8	101.3	26.54	1.688	2.650			
Methane (CH_4)			0.62334	54.0	73.8	46.47	(2.417)	(0.667)	90.68	111.7	[444.]
Ethane (C_2H_6)			0.59861	55.0	75.9	45.66	(2.304)	(1.263)	90.36	184.5	
Propane (C_3H_8)			0.58962	55.3	76.7	45.37	(2.262)	0.493(1.868)	85.52	231.0	
Butane (C_4H_{10})			0.59497	55.5	77.1	45.23	(2.278)	(2.489)	134.9	272.6	
Octane (C_8H_{18})			0.57778	55.8	77.8	45.00	2.123	0.703	214.4	398.8	
Paraffin ($CH_3(CH_2)_{n\approx 23}CH_3$)			0.57275	56.0	78.3	44.85	2.088	0.930			
Nylon (type 6, 6/6)			0.54790	57.5	81.6	41.92	1.973	1.18			
Polycarbonate (Lexan)			0.52697	58.3	83.6	41.50	1.886	1.20			
Polyethylene ($[CH_2CH_2]_n$)			0.57034	56.1	78.5	44.77	2.079	0.89			
Polyethylene terephthalate (Mylar)			0.52037	58.9	84.9	39.95	1.848	1.40			
Polyimide film (Kapton)			0.51264	59.2	85.5	40.58	1.820	1.42			
Polymethylmethacrylate (acrylic)			0.53937	58.1	82.8	40.55	1.929	1.19			1.49
Polypropylene			0.55998	56.1	78.5	44.77	2.041	0.90			
Polystyrene ($[C_6H_5CHCH_2]_n$)			0.53768	57.5	81.7	43.79	1.936	1.06			1.59
Polytetrafluoroethylene (Teflon)			0.47992	63.5	94.4	34.84	1.671	2.20			
Polyvinyltoluene			0.54141	57.3	81.3	43.90	1.956	1.03			1.58
Aluminum oxide (sapphire)			0.49038	65.5	98.4	27.94	1.647	3.970	2327.	3273.	1.77
Barium flouride (BaF_2)			0.42207	90.8	149.0	9.91	1.303	4.893	1641.	2533.	1.47
Bismuth germanate (BGO)			0.42065	96.2	159.1	7.97	1.251	7.130	1317.		2.15
Carbon dioxide gas (CO_2)			0.49989	60.7	88.9	36.20	1.819	(1.842)			[449.]
Solid carbon dioxide (dry ice)			0.49989	60.7	88.9	36.20	1.787	1.563	Sublimes at 194.7 K		
Cesium iodide (CsI)			0.41569	100.6	171.5	8.39	1.243	4.510	894.2	1553.	1.79
Lithium fluoride (LiF)			0.46262	61.0	88.7	39.26	1.614	2.635	1121.	1946.	1.39
Lithium hydride (LiH)			0.50321	50.8	68.1	79.62	1.897	0.820	965.		
Lead tungstate ($PbWO_4$)			0.41315	100.6	168.3	7.39	1.229	8.300	1403.		2.20
Silicon dioxide (SiO_2, fused quartz)			0.49930	65.2	97.8	27.05	1.699	2.200	1986.	3223.	1.46
Sodium chloride (NaCl)			0.47910	71.2	110.1	21.91	1.847	2.170	1075.	1738.	1.54
Sodium iodide (NaI)			0.42697	93.1	154.6	9.49	1.305	3.667	933.2	1577.	1.77
Water (H_2O)			0.55509	58.5	83.3	36.08	1.992	1.000	273.1	373.1	1.33
Silica aerogel			0.50093	65.0	97.3	27.25	1.740	0.200	(0.03 H_2O, 0.97 SiO_2)		

PARTICLE DETECTORS, ABSORBERS, AND RANGES*

A. DETECTOR PARAMETERS

In this section we give various parameters for common detectors. The quoted numbers represent at best *an order of magnitude*, and are useful only for preliminary design. A more detailed introduction to detectors can be found in "A Consumer's Guide to Particle Detectors," by D.J. Miller, Rutherford Lab Report RL-76-072, July 1976.

A.1 Scintillators: Photon yield $\approx 1\gamma/100$ eV in plastic scintillator[1] and $\approx 1\gamma/25$ eV in NaI.[1,2]

A.2 Cerenkov:[3] Half-angle θ_c of cone aperture in terms of velocity β and index of refraction n:

$$\theta_c = \arccos\left(\frac{1}{\beta n}\right) \sim \left[2\left(1-\frac{1}{\beta n}\right)\right]^{1/2}.$$

Threshold velocity: $\beta_t = 1/n$; $\gamma_t = 1/\sqrt{1-\beta_t^2}$.

Therefore, $\beta_t\gamma_t = 1/\sqrt{2\delta+\delta^2}$, where $\delta = n-1$. Values of δ for various commonly used gases are given as a function of pressure and wavelength in Ref. 4; for values at atmospheric pressure, see the Table of Atomic and Nuclear Properties, following.

Number of photons, N, per cm:

$$N = \frac{\alpha}{c}\int\left(1-\frac{1}{\beta^2 n^2}\right)2\pi d\nu = \frac{\alpha}{c}\beta_t^2\int\left(\frac{1}{\beta_t^2\gamma_t^2}-\frac{1}{\beta^2\gamma^2}\right)2\pi d\nu$$

$$\approx 500\sin^2\theta_c/\text{cm (visible spectrum)}.$$

A.3 Photon Collection: In addition to the photon yield, one should take into account the light collection efficiency ($\lesssim$10% for typical 1-cm-thick scintillator), attenuation length ($\approx$1 to 4 m for typical scintillators[5]), and quantum efficiency of the photomultiplier cathode ($\lesssim$25%).

A.4 Typical Detector Characteristics:

Detector Type	Accuracy (rms)	Resolution Time	Dead Time
Bubble chamber	$\approx\pm10$ to $\approx\pm150\mu$	$\approx$ 1 ms	$\approx$1/20 s[a]
Streamer chamber	$\pm300\mu$	$\approx$ 2 μs	$\approx$100 ms
Optical spark chamber	$\pm200\mu$[b]	$\approx$ 2 μs	$\approx$ 10 ms
Magnetostrictive spark chamber	$\pm500\mu$	$\approx$ 2 μs	$\approx$ 10 ms
Proportional chamber	$\gtrsim\pm300\mu$[c,d]	$\approx$ 50 ns	$\approx$200 ns
Drift chamber	±50 to 300μ	$\approx$ 2 ns[e]	$\approx$100 ns
Scintillator	--	$\approx$150 ps	$\approx$ 10 ns
Emulsion	$\pm1\mu$	--	--

[a] Multiple pulsing time.
[b] 60μ for high pressure.
[c] 300μ is for 1 mm pitch.
[d] Delay line cathode readout can give $\pm150\mu$ parallel to anode wire.
[e] For two chambers.

A.5 Shower Detectors: Typical energy resolutions (FWHM) for incident electron in the 1 GeV range, E in GeV. For a fixed number of radiation lengths, FWHM in the last three detectors would be expected to be proportional to $\sqrt{t}$ for t (= plate thickness) $\geq$ 0.2 radiation lengths.[6]

NaI (20 rad. lengths):[7] $\frac{2\%}{E^{1/4}}$

Lead Glass (14 rad. lengths):[8] $\frac{10-12\%}{\sqrt{E}}$

Lead-Liquid Argon (15.75 rad. lengths):[6] $\frac{16\%}{\sqrt{E}}$
(42 cells: 1.1 mm lead, 2 mm liquid argon, 2.3 mm lead-G10, 2 mm liquid argon)

Lead-Scintillator Sandwich (12.5 rad. lengths):[9] $\frac{17\%}{\sqrt{E}}$
(66 cells: 1 mm lead, 5 mm scintillator)

Proportional Wire Shower Chamber (17 rad. lengths):[10] $\frac{40\%}{\sqrt{E}}$
(36 cells: 0.474 rad. length type-metal + Al, 9.5 mm 80% Ar - 20% CH_4 gas)

A.6. Proportional Chamber Wire Instability: The limit on the voltage V for a wire tension T, due to mechanical effects when the electrostatic repulsion of adjacent wires exceeds the restoring force of wire tension, is given by[11]

$$V \leq \frac{sT^{1/2}}{\ell C}$$

where s, ℓ, and C are the wire spacing, length, and capacitance per unit length. An approximation to C for chamber half-gap t and wire diameter d (good for $s \lesssim t$) gives[12]

$$V \lesssim 59T^{1/2}\left[\frac{t}{\ell}+\frac{s}{\pi\ell}\ln\left(\frac{s}{\pi d}\right)\right],$$

where V is in kV, and T is in grams.

A.7 Proportional and Drift Chamber Potentials: Potential distributions and fields for an array of parallel line charges q (coul./m) along z and located at y = 0, x = 0, $\pm a$, $\pm 2a$,..., can usually be calculated with good accuracy from (MKSA):

$$V(x,y) = -\frac{q}{4\pi\epsilon_0}\ln\left\{4\left[\sin^2\left(\frac{\pi x}{a}\right)+\sinh^2\left(\frac{\pi y}{a}\right)\right]\right\}.$$

B. COSMIC RAY FLUXES

The fluxes of particles of different types depend on the latitude, their energy, and the conditions of measurement. Some typical sea-level values[13] for charged particles are given below:

- I_v flux per unit solid angle about vertical direction crossing unit horizontal area
- J_1 perpendicular component of total flux crossing unit horizontal area from above
- J_2 total flux crossing unit horizontal area

	Total Intensity	Hard Component	Soft Component	
I_v	1.1×10^{-2}	0.8×10^{-2}	0.3×10^{-2}	$cm^{-2}\,sec^{-1}\,sterad^{-1}$
J_1	1.8×10^{-2}	1.3×10^{-2}	0.5×10^{-2}	$cm^{-2}\,sec^{-1}$
J_2	2.4×10^{-2}	1.7×10^{-2}	0.7×10^{-2}	$cm^{-2}\,sec^{-1}$

Very approximately, about 75% of all particles at sea-level are penetrating, and are muons. The absolute flux of protons at sea-level, in a momentum range 700-1100 MeV/c, is 1.5×10^{-5} $cm^{-2}\,sec^{-1}\,sterad^{-1}$, or $\sim$0.1% of all particles.

The muon flux at sea-level has a mean energy of 2 GeV and a differential spectrum falling as E^{-2}, steepening smoothly to $E^{-3.6}$ above a few TeV. The angular distribution is $\cos^2\theta$, changing to $\sec\theta$ at energies above a TeV, where θ is the zenith angle at production. The +/- charge ratio is 1.25-1.30. The mean energy of muons originating in the atmosphere is roughly 300 GeV at slant depths $\gtrsim$ a few hundred meters. Beyond slant depths of $\sim$10 km water-equivalent, the muons are due primarily to in-the-earth neutrino interactions (roughly 1/8 interaction $ton^{-1}\,year^{-1}$ for $E_\nu > 300$ MeV, $\sim$ constant throughout the earth).[14] Muons from this source arrive with a mean energy of 20 GeV, and have a flux of 2×10^{-13} $cm^{-2}\,sec^{-1}\,sterad^{-1}$ in the vertical direction and about twice that in the horizontal,[15] down at least as far as the deepest mines.

C. PASSAGE OF PARTICLES THROUGH MATTER

C.1 Energy Loss Rates for Heavy Charged Projectiles: A heavy projectile (much more massive than an electron) of charge $Z_{inc}e$, incident at speed βc ($\beta \gg 1/137$) through a slowing medium, dissipates energy principally via interactions with the electrons of the medium. The mean rate of such energy loss per unit path length x may be written as:[16]

$$\left(\frac{dE}{dx}\right)_{inc} = \frac{D\,Z_{med}\,\rho_{med}}{A_{med}}\left(\frac{Z_{inc}}{\beta}\right)^2$$
$$\times\left[\ln\left(\frac{2m_e\gamma^2\beta^2c^2}{I}\right)-\beta^2-\frac{\delta}{2}-\frac{c}{Z_{med}}\right]\left\{1+\nu\right\},$$

PARTICLE DETECTORS, ABSORBERS, AND RANGES (Cont'd)

where $D = 4\pi N_A r_e^2 m_e c^2 = 0.3070$ MeV cm^2/g (see Physical and Numerical Constants Table).

Here Z_{med} and A_{med} are the charge and mass numbers of the medium and ρ_{med} is the mass density of the medium; I, δ, C, and ν are phenomenological functions. Frequently, the values of δ, C, and ν are negligibly small; the parameter I characterizes the binding of the electrons of the medium. As a rule of thumb, we may estimate I for an idealized medium as $I \simeq 16\ (Z_{med})^{0.9}$ eV when $Z_{med} > 1$. For realistic media the value of I will vary at the 10% level from this estimate; for H_2, $I = 20.0$ eV. We may approximately treat media which are chemical mixtures or compounds by computing

$$\frac{dE}{dx} \approx \sum_{n=1}^{N} \left(\frac{dE}{dx} \right)_n ,$$

with $(dE/dx)_n$ appropriate to the n^{th} chemical constituent (using $\rho_{med}^{(n)}$ as the partial density in the formula for dE/dx).[17]

The function δ represents the density effect upon the energy loss rate; it is non-negligible only for highly relativistic projectiles in denser media.[18] For ultra-relativistic projectiles, δ approaches $2\,\ell n\gamma$ + constant, where the value of the constant depends upon the density of the medium as well as its chemical composition.

The function C represents shell corrections to the energy loss rate.[16] These effects are non-negligible only for projectiles with speeds not much faster than the speeds of the fastest electrons bound in the medium.

The function ν represents corrections due to higher-order electrodynamics.[19] These effects become important when $|Z_{inc}/\beta|$ is comparable to 137. For relativistic unit-charge projectiles, $|\nu|$ is of the order of 1%; positively charged projectiles lose energy more rapidly than do their charge conjugates.[19,20]

For non-relativistic projectiles, our formulae above are inapplicable. At the very slowest speeds, total energy loss rates are believed to be proportional to β, rising through a peak at projectile speeds comparable to atomic speeds, after having passed through a smaller peak (due to elastic Coulomb collisions with the *nuclei* of the slowing medium[21]) at intermediate speeds. In some cases, energy loss rates depend significantly upon the relation of the projectile trajectory to the crystalline structure of the slowing medium.[22]

For relativistic projectiles, $(dE/dx)_{inc}$ falls rapidly with increasing β until reaching a minimum around $\beta = 0.96$ (almost independent of medium), followed by a slow rise. Because of the density effect, the quantity in square brackets approaches $\ell n\gamma$ + constant for large γ.

The quantity $(dE/dx)_{inc}\delta x$ is the *mean* total energy loss via interactions with electrons of the medium in a layer of thickness δx. For any finite δx, Poisson fluctuations can cause the actual energy loss to deviate from the mean. For thin layers, the distribution is broad and skewed, being peaked below $(dE/dx)\delta x$, and having a long tail toward large energy losses.[23] Only for a very thick layer [$(dE/dx)\delta x \gg 2m_e\beta^2\gamma^2c^2$] will the distribution of energy losses become nearly Gaussian. The large fluctuations of the total energy loss rate from the mean are due to a small number of collisions involving large energy transfers. The fluctuations are greatly reduced for the so-called restricted energy loss rate, described in Section C.4.

C.2 Ionization Yields: Physicists frequently relate total energy loss to the number of ion pairs produced in the stopping medium. This relation becomes complicated for relativistic projectiles due to the wandering of energetic knock-on electrons whose ranges exceed the dimensions of the fiducial volume. For a qualitative appraisal of the non-locality of energy deposition by such modestly energetic knock-on electrons in various media, see Ref. 24. The mean energy loss per ion pair produced, W, is essentially constant for relativistic projectiles, but increases at slow projectile speeds.[25] The numerical value of W for gases can be surprisingly sensitive to trace amounts of various contaminants.[25] Of course, in addition to the preceding effects, practical ionization yields may be greatly influenced by subsequent recombinations, etc. [26]

C.3 Energetic Knock-On Electrons: For a relativistic spinless point-charge projectile, the production of high energy (kinetic energy $T \gg I$) electrons is given by (neglecting the spin of the electron):

$$\frac{d^2N}{dTdx} = \frac{1}{2}D \left(\frac{Z_{med}}{A_{med}} \right) \left(\frac{Z_{inc}}{\beta} \right)^2 \rho_{med} \frac{1}{T^2} ,$$

for $I \ll T \leq T_{max}$, where

$$T_{max} = \frac{2m_e\beta^2\gamma^2c^2}{1 + 2\gamma \frac{m_e}{M_{inc}} + \left(\frac{m_e}{M_{inc}} \right)^2} ,$$

M_{inc} is the mass of the incident projectile, and all other quantities are as in Section C.1. This formula does not differ significantly from the precise result, incorporating spin effects, for any projectile (including $e^{\pm}$) in the restricted range $I \ll T \ll T_{max}$; more accurate formulae are available for various projectiles.[27,28] Our formula is inaccurate for T close to I; for $2I \lesssim T \lesssim 10I$, the $1/T^2$ dependence above becomes $\simeq T^{-\eta}$ with $3 \lesssim \eta \lesssim 5$.[29]

C.4 Rates of Restricted Energy Loss for Relativistic Charged Projectiles: The variability of energy loss for heavy projectiles is due primarily to the variability in the production of energetic knock-on electrons. Bremsstrahlung and pair-production processes make this variability even greater for electrons than for heavy particles as projectiles (see, e.g., the figure "Fractional Energy Loss for e^+ and e^- in Lead," following). If an instrument, such as a bubble chamber, is capable of isolating these high-energy-loss interactions, then it is appropriate to consider the rate of energy loss excluding them, i.e., a restricted energy loss rate. The mean energy loss rate via all collisions which have energy transfer T such that $T \leq E_{max} \ll T_{max}$ is:[16]

$$\left(\frac{dE}{dx} \right)_{\leq E_{max}} = \frac{1}{2}D \frac{Z_{med}\rho_{med}}{A_{med}} \left(\frac{Z_{inc}}{\beta} \right)^2 \times \left[\ell n \left(\frac{E_{max}T_{max}}{I^2} \right) - \beta^2 - \delta - \frac{2C}{Z_{med}} \right] .$$

Notice the overall factor of 1/2.

The density effect causes the restricted energy loss rate to approach a constant, the Fermi plateau value, for the fastest projectiles.

C.5 Multiple Scattering through Small Angles: As a charged particle traverses a medium it is deflected by many small-angle elastic scatterings. The bulk of this deflection is due to elastic Coulomb scattering from the nuclei within the medium, hence the usual identification as multiple Coulomb scattering (note, however, that strong interactions do contribute to the total multiple scattering for hadronic projectiles). For both Coulomb and strong interactions, the Central Limit Theorem provides little useful guidance in establishing the precise nature of the distribution of the total deflections resulting from multiple scattering. The true distribution is roughly Gaussian only for small deflection angles while it shows much greater probability for large-angle scatterings $\gtrsim$ a few θ_0, see below, depending on absorber) than the Gaussian would suggest. These tails on the distribution (a few % of peak height in the region where the Gaussian part becomes negligible) are more pronounced for hadrons than for muons as projectiles. The large-angle behavior of these distributions is best estimated by computing the exact distribution for the vectorial sum of the largest deflections based upon the true elastic scattering cross section of the projectile against the medium,[30] or, when applicable, by interpolation from tabular data.[31] An easier alternative which may suffice for non-critical applications would be to use a Gaussian approximation with the following width:[32]

$$\theta_0 = \frac{14.1\ \text{MeV/c}}{p\beta} Z_{inc} \sqrt{L/L_R} \left[1 + \frac{1}{9} \log_{10} \left(L/L_R \right) \right] \text{(radians)},$$

PARTICLE DETECTORS, ABSORBERS, AND RANGES (Cont'd)

where p, β, and Z_{inc} are the momentum (in MeV/c), velocity, and charge number of the incident particle, and L/L_R is the thickness, in radiation lengths, of the scattering medium. L_R for certain materials is given in the Table of Atomic and Nuclear Properties of Materials (following). The angle, θ_0, is a fit to Moliere[30] theory, accurate to about 5% for $10^{-3} < L/L_R < 10$ except for very light elements or low velocity where the error is about 10 to 20%. In this Gaussian approximation, θ_0 has the meaning

$$\theta_0 = \theta_{plane}^{rms} = \frac{1}{\sqrt{2}}\,\theta_{space}^{rms}.$$

The non-projected (space) and projected (plane) angular distributions are given approximately[30] by the Gaussian forms:

$$\frac{1}{2\pi\theta_0^2}\exp\left(-\frac{\theta_{space}^2}{2\theta_0^2}\right)d\Omega,$$

$$\frac{1}{\sqrt{2\pi}\,\theta_0}\exp\left(-\frac{\theta_{plane}^2}{2\theta_0^2}\right)d\theta_{plane},$$

where θ is the deflection angle.

Other quantities are sometimes used to describe the amount of multiple Coulomb scattering: the auxiliary quantities ψ_{plane}, y_{plane}, and s_{plane} (see the figure) obey:

$$y_{plane}^{rms} = \frac{1}{\sqrt{3}}\,L\,\theta_{plane}^{rms} = \frac{1}{\sqrt{3}}L\theta_0,$$

$$\psi_{plane}^{rms} = \frac{1}{\sqrt{3}}\,\theta_{plane}^{rms} = \frac{1}{\sqrt{3}}\theta_0,$$

and

$$s_{plane}^{rms} = \frac{1}{4\sqrt{3}}\,L\,\theta_{plane}^{rms} = \frac{1}{4\sqrt{3}}L\theta_0.$$

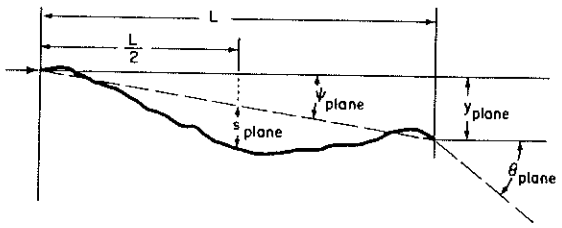

All the quantitative estimates in this section apply only in the limit of small θ_{plane}^{rms} and in the absence of large-angle scatters.

C.6 Longitudinal Distribution of Electromagnetic Showers: A photon of energy E (GeV) $\geq$ 0.1 GeV converting in a semi-infinite medium produces an electromagnetic cascade whose intensity initially increases with depth and then falls off. The average number of $e^{\pm}$ with kinetic energy above 1.5 MeV, crossing a plane at a depth of t radiation lengths from the beginning of the medium, in a material of atomic number Z, calculated using the Monte Carlo program EGS,[33] can be fit by the empirical formula[34]

$$N = N_0 t^a e^{-bt},$$

where $N_0 = 5.51\ E\ \sqrt{Z}\ b^{a+1}/\Gamma(a+1)$ and $b = 0.634 - 0.0021\ Z$. For $Z \geq 26$, $a = 2.0 - Z/340 + (0.664 - Z/340)\ \ell n\ E$. For $Z = 13$, $a = 1.77 - 0.52\ \ell n\ E$. The maximum intensity, N_{max}, occurs at the depth $t = a/b$. The maximum error of the fit occurs in the vicinity of this depth and is less than $0.15\ N_{max}$. The integral of the tail, $\int_{1.5\ a/b}^{\infty} N\,dt$ is fit to better than 2.5%. The total longitudinally-projected $e^{\pm}$ path length, $\int_0^{\infty} N\,dt = 5.51\ E\ \sqrt{Z}$, is less than the total $e^{\pm}$ path length due primarily to multiple Coulomb scattering.

---

*Prepared April 1974 by Sherwood Parker and Bernard Sadoulet. Revised April 1982 by Sherwood Parker, Ray Hagstrom, Didier Besset, and John Learned.

1. *Methods of Experimental Physics*, L.C.L. Yuan and C.-S. Wu, editors, Academic Press, 1961, Vol. 5A, p.127.
2. R.K. Swank, Ann. Rev. Nucl. Sci. **4**, 137 (1954), and G.T. Wright, Proc. Phys. Soc. **B68**, 929 (1955).
3. *Methods of Experimental Physics*, L.C.L. Yuan and C.-S. Wu, editors, Academic Press, 1961, Vol. 5A, p.163.
4. E.R. Hayes, R.A. Schluter, and A. Tamosaitis, "Index and Dispersion of Some Cerenkov Counter Gases," ANL-6916 (1964).
5. Nuclear Enterprises Catalogue.
6. D. Hitlin et al., Nucl. Instr. and Meth. **137**, 225 (1976). See also W.J. Willis and V. Radeka, Nucl. Instr. and Meth. **120**, 221 (1974), for a more detailed discussion.
7. E.B. Hughes et al., IEEE Transactions on Nuclear Science **NS-19**, No. 3, 126 (1972).
8. M. Holder et al., Phys. Letters **40B**, 141 (1972), and J.S. Beale et al., "A Lead-Glass Cerenkov Detector for Electrons and Photons," CERN Writeup, Intl. Conf. on Instrumentation in H.E.P., Frascati (1973).
9. W. Hofmann et al., DESY 81/045 (July 1981). See also S.L. Stone et al., Nucl. Instr. and Meth. **151**, 387 (1978).
10. R.L. Anderson et al., "Tests of Proportional Wire Shower Counter and Hadron Calorimeter Modules," SLAC-PUB-2039 (1977).
11. T. Trippe, CERN NP Internal Report 69-18 (1969).
12. S. Parker and R. Jones, LBL-797 (1972), and A. Morse and B. Feshbach, *Methods of Theoretical Physics*, McGraw-Hill, New York, 1953, p.1236.
13. B. Rossi, Rev. Mod. Phys. **20**, 537 (1948).
14. J.G. Learned, F. Reines, and A. Soni, Phys. Rev. Lett. **43**, 907 (1979).
15. M.F. Crouch et al., Phys. Rev. **D18**, 2239 (1978).
16. U. Fano, Ann. Rev. Nucl. Sci. **13**, 1 (1963).
17. H.A. Bethe and J. Ashkin, *Experimental Nuclear Physics*, Vol. 1, E. Segrè, editor, John Wiley, New York, 1959.
18. A. Crispin and G.N. Fowler, Rev. Mod. Phys. **42**, 290 (1970).
19. For Z^3 calculations with Z = 1, see J.D. Jackson and R.L. McCarthy, Phys. Rev. **B6**, 4131 (1972).
20. For an approximate treatment of high-Z projectiles, see P.B. Eby and S.H. Morgan, Phys. Rev. **A5**, 2536 (1972).
21. See, for instance, G. Sidenius, Det Kong. Danske Viden. Selskab Mat.-Fysk. Med. **39**, No. 4 (1974).
22. See, for instance, S. Datz, "Atomic Collisions in Solids" in "Structure and Collisions of Ions and Atoms," Springer Verlag, Berlin, 1978, p. 309.
23. See, for instance, K.A. Ispirian, A.T. Margarian, and A.M. Zverev, Nucl. Instr. and Meth. **117**, 125 (1974).
24. L.V. Spencer "Energy Deposition by Fast Electrons," Nat'l Bureau of Standards Monograph No. 1 (1959).
25. "Average Energy Required to Produce an Ion Pair," ICRU Report No. 31 (1979).
26. N. Hadley et. al, "List of Poisoning Times for Materials," TPC-LBL-79-8 (1981).
27. For unit-charge projectiles, see E.A. Uehling, Ann. Rev. Nucl. Sci. 4, 315 (1954).
28. For highly charged projectiles, see J.A. Doggett and L.V. Spencer, Phys. Rev. **103**, 1597 (1956). A Lorentz transformation is needed to convert these center-of-mass data to knock-on energy spectra.
29. N.F. Mott and H.S.W. Massey, *The Theory of Atomic Collisions*, Oxford Press, London, 1965.
30. For a thorough discussion of simple formulae for single scatters and methods of compounding these into multiple-scattering formulae, see W.T. Scott, Rev. Mod. Phys. **35**, 231 (1963). For detailed summaries of formulae for computing single scatters, see J.W. Motz, H. Olsen, and H.W. Koch, Rev. Mod. Phys. **36**, 881 (1964).
31. E.V. Hungerford and B.W. Mayes, Atomic Data and Nuclear Data Tables **15**, 477 (1975).
32. V.L. Highland, Nucl. Inst. and Meth. **129**, 497 (1975) and important modification Nucl. Inst. and Meth. **161**, 171 (1979).
33. R. Ford and W. Nelson, SLAC-210 (1978).
34. A similar form has been used by E. Longo and I. Sestili, Nucl. Inst. and Meth. **128**, 283 (1975), and J. Sass and M. Spiro, CERN $\bar{p}p$ Tech. Note 78-32 (1978).